Effect of Cationic Brush-Type Copolymers on the Colloidal Stability of GdPO$_4$ Particles with Different Morphologies in Biological Aqueous Media

Vaidas Klimkevicius,[§] Matas Janulevicius,[§] Aleksandra Babiceva, Audrius Drabavicius, and Arturas Katelnikovas*

ACCESS | Metrics & More | Article Recommendations | SI Supporting Information

ABSTRACT: In this study, we present the synthesis of cationic brush-type polyelectrolytes and their use in the stabilization of GdPO$_4$ particles in aqueous media. Polymers of various compositions were synthesized via the RAFT polymerization route. SEC equipped with triple detection (RI, DP, RALS, and LALS) was used to determine the molecular parameters (M_n, M_w, M_w/M_n). The exact composition of synthesized polymers was determined using NMR spectroscopy. Cationic brush-type polymers were used to improve the stability of aqueous GdPO$_4$ particle dispersions. First, the IEPs of GdPO$_4$ particles with different morphologies (nanorods, hexagonal nanoprisms, and submicrospheres) were determined by measuring the zeta potential of bare particle dispersions at various pH values. Afterward, cationic brush-type polyelectrolytes with different compositions were used for the surface modification of GdPO$_4$ particles (negatively charged in alkaline media under a pH value of ~10.6). The concentration and composition effects of used polymers on the change in particle surface potential and stability (DLS measurements) in dispersions were investigated and presented in this work. The most remarkable result of this study is redispersible GdPO$_4$ nanoparticle colloids with increased biocompatibility and stability as well as new insights into possible cationic brush-type polyelectrolyte applicability in both scientific and commercial fields.
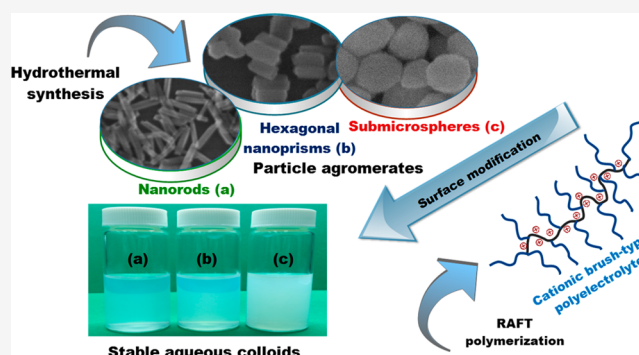
INTRODUCTION

The development of various novel nanomaterials and nanostructures is among the most rapidly progressing fields in a modern science. Due to their unique properties, which emerge as the size of the particle or structure decreases to the nanoscale, nanomaterials, regarding the application, frequently are far superior to micro- and macromaterials.[1−4] Newly developed functional nanomaterials often offer revolutionary properties and therefore are successfully applied in chemical, technological, biological, medical, and other fields.[5−9]

Most scientific papers, reporting the development of nanoparticles, claim possible nanoparticle applicability in fields which require colloidal stability (nanoparticles for biomedical applications, etc.). Colloidal stability (preferably over a wide pH range, including biological systems) is a crucial parameter and limiting factor in overall nanoparticle applicability in the mentioned fields because living organisms are commonly water-based.[10−14] Typically, nanoparticle colloidal stability is evaluated visually by conducting zeta potential measurements. In the ideal case, zeta potential measurements are supported by DLS experiments. However, such ideal case scenarios of nanoparticle stability evaluation are rather rare. Unfortunately, the authors of papers, despite intended applications, rarely

evaluate the actual colloidal stability in aqueous media at all.[15−18]

Rare-earth-doped nanoparticles are materials of great interest lately.[19,20] The type of nanoparticle which can be excluded from the others would be those containing Gd^{3+} ions in their composition. Gadolinium-based particles can potentially be applied as MRI contrast agents because the Gd^{3+} ion has seven unpaired electrons in its 4f orbital.[21−23] There is plenty of published research regarding the synthesis and investigation of Gd-based nanoparticles such as GdPO$_4$, GdF$_3$, NaGdF$_4$, and Gd$_2$O$_3$. Gd-based nanoparticles are suitable hosts for doping with lanthanide ions in order to enrich these materials with additional luminescence properties.[5,19,20,23−25] One the most widely studied Gd-based particles is NaGdF$_4$ doped with various lanthanide ions. Such particles are often referred to as potential
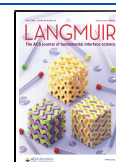
biomarkers in biomedicine.[26−28] However, the commonly used thermal decomposition[29] synthesis method leads to hydrophobic nanoparticles due to employed oleic acid, which remains on the particle surface.[30−32] A hydrophobic surface prevents any colloidal stability of $NaGdF_4$ particles in aqueous media; therefore, a change in surface ligands or additional surface modification is needed in order to achieve the colloidal stability of such particles in aqueous media.[33]

The necessity of novel Gd-based particles, which possess desired properties such as a ligand-free surface, chemical and thermal stability, and biological inertness, still exists. Ortho-phosphates proved to be promising host materials to satisfy such needs.[34−36] One of the approaches to obtaining rare-earth phosphate nanoparticles is hydrothermal synthesis. The main advantages of such a method are its repeatability, possibility to control the growth of the synthesized particles and, most importantly, the fact that it does not require any hydrophobic ligands (e.g., oleic acid).[37,38] Hydrothermally obtained particles typically have ligand-free surfaces and therefore are suitable for further surface modifications. There are numerous papers reporting the hydrothermal synthesis of $GdPO_4$ particles. Many of those claim that $GdPO_4$ particles can be applied in the biomedical field.[39−45] However, due to some limitations, such as reduced colloidal stability in aqueous media, $GdPO_4$ particles are not applied in vivo very frequently.

Recently, a paper reporting the controlled hydrothermal synthesis of $GdPO_4$ particles and their stability investigation was published.[46] It is important to notice that particles reported in this paper can form stable aqueous colloids. However, at neutral pH values all investigated particles are close to their isoelectric point, meaning that the surface charge of the particles is not high enough to ensure the stability of their colloids in aqueous media. Agglomeration, besides the observed $GdPO_4$ stability, remains a limiting factor for such nanoparticle applicability.

The stabilization of nanoparticles prevents the formation of agglomerates. Nanoparticle stability in aqueous colloids can be achieved either electrostatically or sterically. In most cases, electrostatic stabilization, induced by charge repulsion, does not ensure reliable-enough stability and the prevention of agglomeration.[38,47−49] Thus, steric stabilization, achieved by attaching a surfactant to a particle surface (either by chemical bonds or by electrostatic interactions), is more effective because the created steric barriers prevent particles from approaching an agglomerate too closely.[50,51] In order to apply any nano- or microsized particles, for example, $GdPO_4$ mentioned above, in fields which require superior colloidal stability (e.g., as nanoprobes), it is necessary to additionally enhance the particle stability. For this reason, various low-molecular-weight surfactants such as TWEEN, CTAB, and TRITON are used to enhance the stability of various nanoparticle systems.[23,39,52−55] Even though the use of various commercial surfactants often prevents particles from agglomerating, such surface modification cannot always ensure the desired stability of nanoparticles, especially in water. There is currently no effective universal way to ensure the colloidal stability of various nano- and microsized particles in aqueous colloids.

We believe that a viable solution for the discussed issues could be the use of cationic brush-type polymers. It is already known that polymeric brush-type electrolytes have a high potential for the surface modification and stabilization of nanoparticles (e.g., SiO_2, TiO_2).[51,56,57] In fact, studies show that the use of such brush-type polymers for the stabilization of particles is a more effective approach than using low-molecular-weight equivalents.

However, no study on the stabilization of various morphology nanoparticles of the same crystalline phase using similar brush-type polymers exists.

In this work, we demonstrate a successful stabilization of $GdPO_4$ nanoparticles with different morphologies (nanorods, hexagonal nanoprisms, and submicrospheres) using cationic brush-type polyelectrolytes with different charge densities. The focus of this research was to investigate and determine the correlation among the zeta potential of $GdPO_4$ particles with different morphologies, the quantitative adsorption of different custom-made cationic brush-type copolymers on the particle surface, and the overall stability of $GdPO_4$ particle colloids. Redispersible $GdPO_4$ nanoparticle colloids with increased colloidal stability were obtained during this study. Not only the stability in aqueous media but also the biocompatibility of $GdPO_4$ particles is greatly enhanced after the surface modification with the p($METAC$-*stat*-$PEO_{19}MEMA$) polyelectrolyte. The enhanced biocompatibility is due to PEO chains originating from p($METAC$-*stat*-$PEO_{19}MEMA$). $GdPO_4$ particles are also suitable hosts for doping with rare-earth ions to enrich them with luminescence. We believe previously discussed benefits, such as increased nanoparticle stability and redispersibility from dry powder, suggest that the p($METAC$-*stat*-$PEO_{19}MEMA$) polyelectrolyte, along with similar cationic brush-type polymers, can successfully be applied in both biomedical and commercial fields.

■ EXPERIMENTAL SECTION

Materials. Poly(ethylene glycol) methyl ether methacrylate ($PEO_{19}MEMA$, M_n 950, Aldrich) and [2-(methacryloyloxy)ethyl] trimethylammonium chloride (METAC, 80% aqueous solution, Aldrich) were purified of inhibitors by passing the monomers through a column filled with basic alumina (type 5016A, Fluka). Methanol (MeOH, 99.8%, Aldrich), acetone (99%, Aldrich), ethylene glycol (EG, 99.5%, Fluka), diethyl ether (Et_2O, 99%, Aldrich), carbon disulfide (CS_2, 99.9%, Aldrich), 1-butanthiol (99%, Aldrich), sodium hydride (NaH, 60% dispersion in mineral oil, Aldrich), iodine (I_2, 99.8%, Aldrich), and 4,4′-azobis(4-cyanovaleric acid) (ACVA, 98%, Fluka) were used as received. Gd_2O_3 (99.99%, Tailorlux), ammonium dihydrogen phosphate ($NH_4H_2PO_4$, 99.9%, EuroChemicals), nitric acid (HNO_3, 70%, EuroChemicals), ammonium hydroxide (NH_4OH, 25%, EuroChemicals), and tartaric acid (99.99%, EuroChemicals) were used as received. $Gd(NO_3)_3$ was prepared by dissolving the required amount of Gd_2O_3 in nitric acid.

Synthesis of $GdPO_4$ Particles with Controlled Different Morphologies. Particles with different morphologies (nanorods, hexagonal nanoprisms, and submicrospheres) were synthesized by a hydrothermal route according to the previously published procedure with minor adjustments.[46] The morphology of synthesized particles was controlled by the variation of the initial molar ratio of Gd^{3+} to $PO_4^{3−}$. The morphological features of synthesized $GdPO_4$ particles were investigated using SEM (Scanning Electron microscopy) and TEM (transmission electron microscopy).

The crystalline phase (hexagonal rhabdophane; PDF ICDD 00-039-0232, space group $P3_121$) of particles was determined using XRD (X-ray powder diffraction) equipment. The synthesis procedure, analysis conditions, and XRD data in detail are provided in the Supporting Information (SI, Figure S1).

Synthesis of Cationic Brush-Type Polyelectrolytes. Cationic brush-type polyelectrolytes p($METAC$-*stat*-$PEO_{19}MEMA$) were prepared via the RAFT (radical addition−fragmentation chain transfer) polymerization method from three different monomer feeds, METAC/$PEO_{19}MEMA$ = 25:75, 45:55, and 65:35 mol %, according to the previously described procedure[51] with minor modifications. (Different chain-transfer agent 4-(((butylthio)carbonothioyl)thio)-4-cyano-pentanoic acid (BCPA) was used). BCPA was freshly synthesized before use according to the published data.[58] The synthesis scheme of
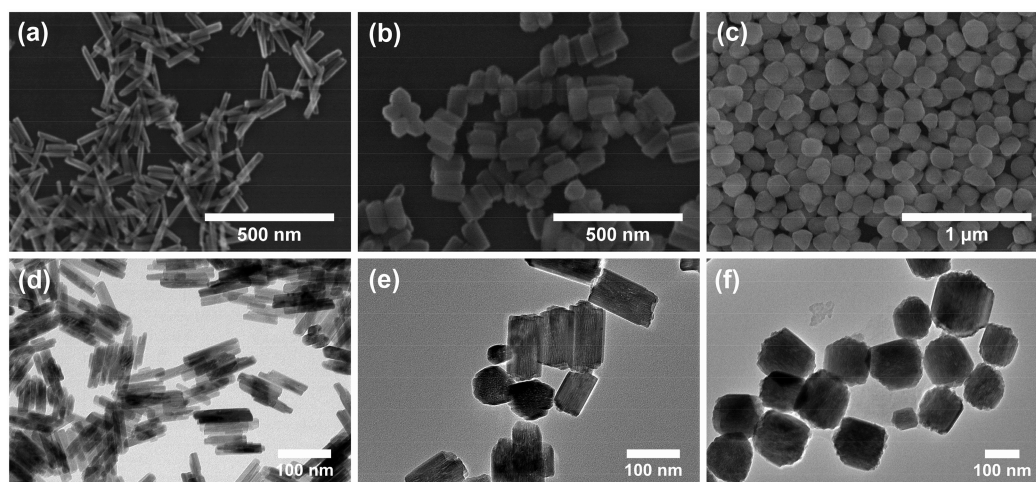
Figure 1. (a−c) SEM and (d−f) TEM images of GdPO$_4$ nanoparticles with different morphologies. Images represent the NH$_4$H$_2$PO$_4$/Gd^{3+} molar ratio impact upon particle morphology: (a, d) 10, (b, e) 50, and (c, f) 100, respectively.

p(METAC-*stat*-PEO$_{19}$MEMA) with different morphologies is provided in Figure 2.
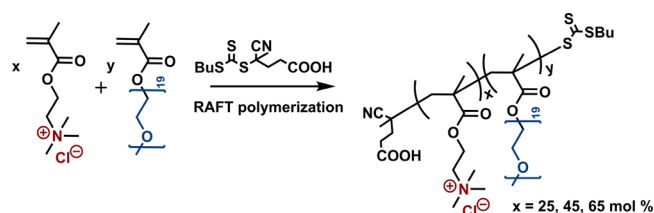
Figure 2. Synthesis scheme of cationic brush-type p(METAC-*stat*-PEO$_{19}$MEMA) polyelectrolytes via the RAFT method.

In all three cases, the molar ratio of initial synthesis components [M]$_0$/[BCPA]$_0$/[ACVA]$_0$ was the same (i.e., equal to 100:3:1, where [M]$_0$ represents the sum of the molar concentrations of both monomers in the reaction feed). RAFT copolymerization of METAC and PEO$_{19}$MEMA was carried out in a round-bottomed flask sealed with a silicone septum under an inert N$_2$ atmosphere in a 70:30 (v/v) mixture of ethylene glycol and water. The polymerization mixtures with an overall 15% monomer concentration were magnetically stirred for 12 h at 70 °C. After synthesis, the mixture was cooled and the flask was opened to air to quench the polymerization. Synthesized polymers were purified by ultrafiltration (10 kDa MWCO) against a 0.15 M NaCl aqueous solution and later against deionized water. Polymer solutions were concentrated using a rotary evaporator and separated by freeze-drying.

The NMR and SEC techniques (detailed analysis conditions in Figures S2 and S3) were applied to determine the composition and exact macromolecular parameters (number average molecular weight (M_n), dispersity ($Đ$), and calculated degrees of polymerization) of the synthesized polymers, respectively. The macromolecular parameter and exact composition of cationic polyelectrolytes used in this study are provided in Table 1.

Preparation of Dispersions. A colloidal 1 or 10 mg/mL dispersion was prepared by dispersing GdPO$_4$ particles with a particular morphology in Milli-Q water. The pH of each suspension was set to 10.6 using 1.0 M and then 0.1 M ammonium hydroxide (NH$_4$OH) solutions. All dispersions were treated with ultrasound in an ultrasonic bath for 15 min to disassemble nanoparticle agglomerates. Afterward, appropriate amounts of cationic brush-type polyelectrolytes p-(METAC-*stat*-PEO$_{19}$MEMA) were added to the dispersion (up to 200 mg of polymer per gram of dry GdPO$_4$ particles) and ultrasonically treated again for 15 min.

Determination of the Isoelectric Point (IEP) of GdPO$_4$ Particles. The IEP point values of bare and modified GdPO$_4$ particles with different morphologies were determined by measuring zeta potentials under different pH values in aqueous dispersions. The pH of GdPO$_4$ dispersions was adjusted from 2 to 10 using 0.1 M HNO$_3$ and 0.1 M NH$_4$OH solutions, respectively. Zeta potential values were measured with a Malvern Zetasizer Nano ZS using the Smoluchowski model at 25 °C.

Determination of Polymer Adsorption and Surface Potential. The adsorbed amount of cationic polyelectrolyte on the surface of GdPO$_4$ particles was evaluated by measuring the change in zeta potential as a function of the amount of polymer added to alkaline aqueous (pH 10.6) dispersions.

The equilibrium polymer adsorption is observed at the point where the value of the zeta potential reached the plateau. Cationic polyelectrolytes with three different compositions were evaluated, and thus the effectiveness of all three polyelectrolytes was compared.

Determination of the Colloidal Stability of Aqueous GdPO$_4$ Dispersions. The colloidal stability of bare and modified GdPO$_4$ dispersions at different pH values was evaluated by measuring the particle size distribution using the dynamic light scattering (DLS) method. DLS measurements were carried out using a ZetaSizer Nano ZS (Malvern) equipped with a 4 mW He−Ne laser emitting at a wavelength of 633 nm. Measurements were performed at 25 °C and an angle of 173° using noninvasive backscattering (NIBS) technology. Using NIBS, the particle size detection range was 0.3 nm−10 μm. The

**Table 1. Characteristics of the Synthesized p(METAC-*stat*-PEO$_{19}$MEMA) Copolymers[a]**

no.	copolymer charge	[METAC]$_0$/ [PEO$_{19}$MEMA]$_0$	M_n, kDa[b]	$Đ$	DP	[METAC]/ [PEO$_{19}$MEMA][c]
1.	low	25:75	28.5	1.15	38	27:73
2.	medium	45:55	24.6	1.16	41	47:53
3.	high	65:35	19.4	1.12	42	65:35

[a]Polymerization conditions: [M]$_0$/[CTA]$_0$/[I]$_0$ = 100:3:1, T = 70 °C, t = 12 h. [b]Determined using size exclusion chromatography (SEC). [c]Calculated from ^{1}H NMR spectra.

size distribution data was analyzed using Zetasizer software from Malvern.

RESULTS AND DISCUSSION

Surface Potential and Colloidal Stability of Bare GdPO₄ Particles with Different Morphologies. The main object of this investigation was $GdPO_4$ particles with three different morphologies (i.e., nanorods, hexagonal nanoprisms, and submicrospheres). The change in the $GdPO_4$ particle surface potential was evaluated by measuring zeta potential values in aqueous colloidal dispersions in the pH range from 2 to 10 (Figure 3a). Zeta potential values of the synthesized $GdPO_4$
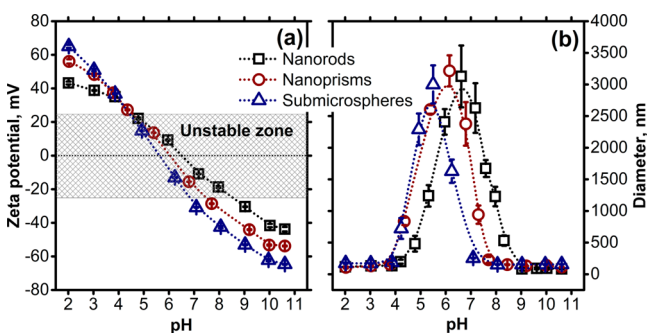
Figure 3. (a) Zeta potential and (b) particle size of bare $GdPO_4$ particles with different morphologies in aqueous dispersions at various pH values: nanorods (□), nanoprisms (○), and submicrospheres (△).

particles slightly differ and are dependent on the particle morphology. For example, the zeta potential value of submicrospheres in aqueous alkaline media (pH 10.6) is −64.7 mV. Under identical conditions, the measured zeta potential values for hexagonal nanoprisms and nanorods are observed to be higher, −53.8 and −43.8 mV, respectively. It is interesting that $GdPO_4$ particles with different morphologies possess different isoelectric points. (The isoelectric point is determined by the pH value, where the zeta potential is equal to 0, which will be referred to as the IEP.) The determined IEP value for nanorods is 6.53. IEP values of hexagonal nanoprisms and submicrospheres are shifted to lower pH values, 6.03 and 5.61, respectively. These differences in IEP could be related to different phosphate group density on differently shaped $GdPO_4$ particle surfaces since the surface potential of the particles is related to the number of surface-exposed PO_4^{3-} groups. The

shape of template $GdPO_4$ particles and therefore the number of such surface-exposed phosphate groups were manipulated by varying the $NH_4H_2PO_4/Gd^{3+}$ molar ratio by employing a hydrothermal synthesis route as reported in the literature.[46] $NH_4H_2PO_4/Gd^{3+}$ molar ratios of 10, 50, and 100 were used for the hydrothermal synthesis of nanorods, hexagonal nanoprisms, and submicrospheres, respectively.

The colloidal stability of bare $GdPO_4$ particles with different morphologies in aqueous media under various pH values was measured using DLS equipment (Figure 3b). Typical unstable zones were observed during stability measurements of bare $GdPO_4$ particle dispersions. Regardless of particle morphology, agglomeration and fast sedimentation of particles in an aqueous dispersion occurred if absolute values of the zeta potentials of particles were lower than |22| mV. Almost identical $GdPO_4$ particle agglomeration and sedimentation due to changes in electric repulsion forces were reported in our earlier studies of particle stabilization.[46]

Surface Modification of Different GdPO₄ Particles Using Cationic Brush-Type Polyelectrolytes in Alkaline Media. For the surface modification of $GdPO_4$, three p(METAC-*stat*-PEO₁₉MEMA) polyelectrolytes with different compositions were synthesized. Different polymer compositions were obtained by the variation of the initial molar ratio of METAC and PEO₁₉MEMA (Table 1). METAC groups contain positively charged quaternary ammonium groups that could electrostatically anchor to the negatively charged surface of $GdPO_4$ particles. Moreover, the PEO₁₉MEMA polymer can be additionally defined as an inert, biocompatible macromonomer containing relatively long PEO substituents. These substituents are responsible for a steric barrier that prevents other particles from approaching too closely; therefore, agglomeration is avoided. PEO-stabilized particles are also known to possess good biocompatibility.[59] According to the number of quaternary ammonium groups in the copolymer composition, different p(METAC-*stat*-PEO₁₉MEMA) copolymers were classified as having low, medium, and high charge, where low means that the copolymer consist of 27 mol %; medium, 47 mol %; and high, 65 mol % METAC groups in composition.

The adsorption of a cationic brush-type polyelectrolyte on oppositely charged surfaces of $GdPO_4$ particles with different morphologies was evaluated by measuring the change in the particle zeta potential. Measurements were carried out in alkaline media (pH 10.6), where $GdPO_4$ particles have a highly
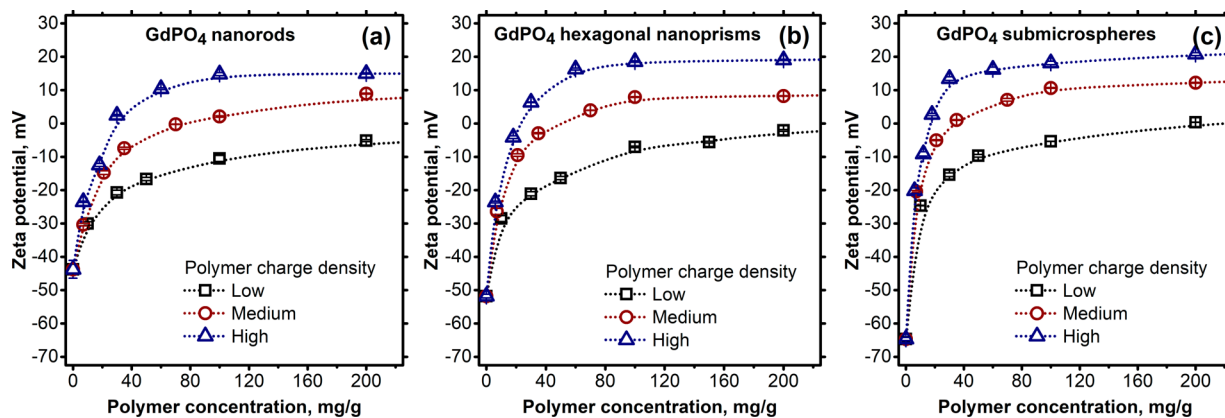
Figure 4. Dependence of the zeta potential of $GdPO_4$ particles in alkaline aqueous media (pH 10.6) as a function of polymer concentration: (a) nanorods, (b) nanoprisms, and (c) submicrospheres.
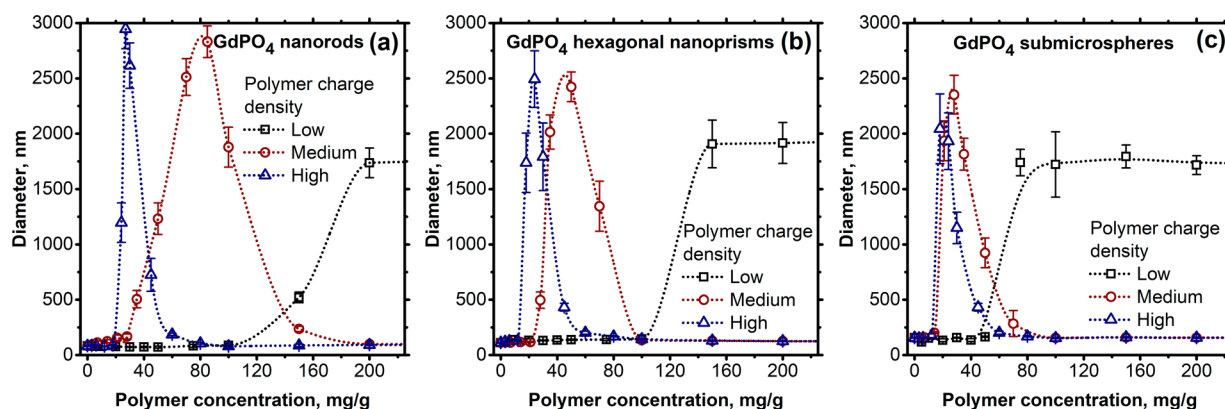
Figure 5. Dependence of the GdPO$_4$ particles size in alkaline aqueous media (pH 10.6) as a function of polymer concentration and polymer charge density: (a) nanorods, (b) nanoprisms, and (c) submicrospheres.

expressed negative charge. The effect of the amount of copolymer on the change in zeta potential of GdPO$_4$ particles with different morphologies in aqueous dispersions is presented in Figure 4.

During the addition of copolymer, the change in the zeta potential value and thus the charge on the GdPO$_4$ particle surface are affected by both the polymer charge density and the particle morphology (Figure 4.). Clearly, the charge density of polymers has a greater effect. For example, during the addition of a low-charge-density polymer to an aqueous dispersion with rod-like GdPO$_4$ nanoparticles, the full charge compensation is not achieved, and the surface of GdPO$_4$ nanorods remains negative (-5.1 mV) even when using a large amount of polymer (200 mg per gram of GdPO$_4$ particles in dispersion). Different behavior was observed using polymers with medium or high charge density. Surface charge inversion was observed during the physical adsorption of polymers with both medium and high densities of positively charged quaternary ammonium groups (METAC units). This behavior is explained in the literature,[51] where similarly structured cationic brush-type polyelectrolytes were applied for the stabilization of TiO$_2$ particles in aqueous media. The charge inversion effect is induced by an excess number of METAC groups on the particle surface during adsorption. The surface charge of GdPO$_4$ nanorods after the addition of medium- and high-density polymers (200 mg/g) reached $+8.9$ and $+15.0$ mV, respectively. Similar effects were observed during the investigation of GdPO$_4$ hexagonal nanoprisms. The zeta potential values of GdPO$_4$ hexagonal nanoprisms treated with low-, medium-, and high-charge p(METAC-*stat*-PEO$_{19}$MEMA) polyelectrolytes (amount of 200 mg/g) reached -2.1, $+8.2$, and $+19.1$ mV, respectively. Different from nanorods and hexagonal nanoprisms, the negatively charged surface of GdPO$_4$ submicrospheres after treatment with polymers was fully compensated for ($+0.35$ mV) using even a low-charge-density (27 mol % charged groups) polyelectrolyte. The medium- and high-charge p(METAC-*stat*-PEO$_{19}$MEMA) polyelectrolytes that were used led to the described charge inversion effect, and the zeta potentials of submicrosphere GdPO$_4$ particles were $+12.2$ and $+20.8$ mV, respectively.

Colloidal stability was evaluated and observed throughout all GdPO$_4$ particle treatment with the p(METAC-*stat*-PEO$_{19}$MEMA) procedure by measuring the particle size distribution (PSD) using dynamic light scattering equipment. A colloidal stability evaluation of differently shaped GdPO$_4$ particles is presented in Figure 5. Note that particles were

treated using three different cationic brush-type polymers with different charge densities (low, medium, and high).

Regardless of the morphology, all GdPO$_4$ particles are stable in alkaline aqueous media (pH 10.6) without added polymer. In such cases, the stability of particles is ensured by electrostatic repulsion forces between highly (negatively) charged particles. Zeta potential values of GdPO$_4$ with the morphology of nanorods, hexagonal nanoprisms, and submicrospheres in alkaline media (pH 10.6) were observed to be -43.8, -53.8, and -64.7 mV, respectively.

The amount of polymer in such dispersions plays an important role. After the addition of a certain amount of polymer, dispersions became unstable. For example, during the treatment of GdPO$_4$ nanorods, particle dispersions were stable for up to 100 mg/g of added low-charge-density polymer. The addition of a larger amount of such a polymer in a dispersion led to the formation of agglomerates of up to 1800 nm. The addition of medium- and high-charge polymers to GdPO$_4$ particle dispersions showed different behavior. In these cases, GdPO$_4$ nanorod dispersions had typical zones of instability if the amount of polymer in the dispersion was insufficient. Instability zones of identical GdPO$_4$ nanorod dispersions stabilized using medium- and high-charge p(METAC-*stat*-PEO$_{19}$MEMA) polymers were determined to be from 30 to 150 and from 20 to 60 mg/g, respectively. In these zones, particles existed in an agglomerated state, and the measured PSD showed values of up to 3000 nm. After increasing the amount of polymer over these ranges, dispersions of GdPO$_4$ nanorods became stable again. The determined PSDs of modified GdPO$_4$ nanorods in alkaline media were $\sim$80 nm using both medium- and high-charge polyelectrolytes. The determined PSD values using DLS were relatively close to those measured using TEM and SEM (Figure 1). The unstable zones that occurred during the study could be related to the particle zeta potential. During treatment with polymers, the change in particle surface potential mainly depends on the amount of polymer added and the density of positively charged quaternary ammonium groups within the polymer itself. It was found that p(METAC-*stat*-PEO$_{19}$MEMA) polymers with a high charge density had the greatest impact on the zeta potential values of GdPO$_4$ particles. A smaller amount of such polymers was needed to reach the same value of the zeta potential in comparison to polyelectrolytes containing a small number of positively charged groups. Similar results were obtained during the stability study of GdPO$_4$ particles with other morphologies (hexagonal nanoprisms and submicrospheres) and are summarized in Table 2. It is important to note that

Table 2. Stability Results of GdPO$_4$ Particles with Different Morphologies during Treatment with Different Polymers in Alkaline Aqueous Media (pH 10.6)

| | nanorods | | hexagonal nanoprisms | | submicrospheres | |
| | unstable zone | | unstable zone | | unstable zone | |
polymer charge density	polymer amount, mg/g	ζ, mV	polymer amount, mg/g	ζ, mV	polymer amount, mg/g	ζ, mV
low	>125	>−8.9	>100	>−8.4	>50	>−8.7
medium	35 to 150	−8.5 to +7.4	22.5 to 100	−8.9 to +7.8	15 to 70	−9.3 to +7.4
high	20 to 60	−9.5 to +10.9	15 to 50	−8.9 to +11.3	12.5 to 45	−9.1 to +11.9

Table 3. Zeta Potential and Calculated Equilibrium Adsorption of Cationic Polyelectrolytes on GdPO$_4$ Particles with Different Morphologies in Alkaline Aqueous Media (pH 10.6)

| | polymer charge density | | | | | | | | |
| | low | | | medium | | | high | | |
GdPO$_4$ morphology	ζ, mV[a]	ζ, mV[b]	equilibrium adsorption, mg/g[c]	ζ, mV[a]	ζ, mV[b]	equilibrium adsorption, mg/g[c]	ζ, mV[a]	ζ, mV[b]	equilibrium adsorption, mg/g[c]
nanorods	−5.2	−17.0	39.2	+8.9	−8.3	36.5	+15.0	+3.2	36.8
hexagonal nanoprisms	−2.1	−23.3	23.0	+8.2	−8.9	21.8	+19.1	+1.0	23.4
submicrospheres	+0.35	−32.3	8.7	+12.2	−17.3	11.1	+20.8	−6.8	13.3

[a]Zeta potential of GdPO$_4$ in alkaline aqueous media (pH 10.6) before washing. [b]Zeta potential of GdPO$_4$ in alkaline aqueous media (pH 10.6) after washing with Milli-Q water (three times). [c]Equilibrium adsorption of p(METAC-*stat*-PEO$_{19}$MEMA) with different charge density on the surface of GdPO$_4$ particles, calculated from the curves presented in Figure 4.
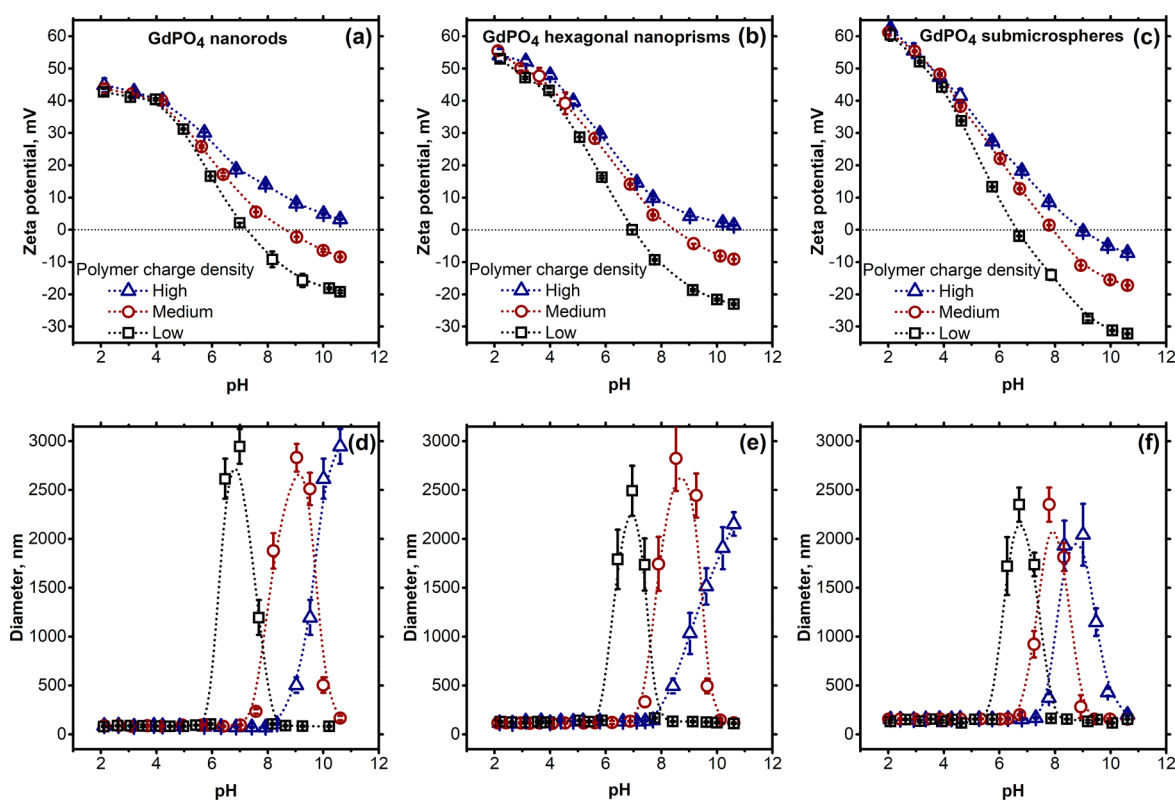
Figure 6. Dependence of the (a−c) zeta potential and (d−f) size of modified GdPO$_4$ particles as a function of the pH of the medium: (a, d) nanorods, (b, e) nanoprisms, and (c, f) submicrospheres.

instability zones of GdPO$_4$ particles, regardless of particle morphology, are observed when the absolute zeta potential value of particles was in the range of |12| mV (Figure 4).

Determination of the Equilibrium Polymer Adsorption of GdPO$_4$ with Different Morphologies. The equilibrium quantity of cationic brush-type polyelectrolyte adsorption on oppositely charged surfaces of GdPO$_4$ particles

with three different morphologies (nanorods, hexagonal nanoprisms, and submicrospheres) was evaluated by measuring zeta potential values of particles treated with 200 mg/g polymers (low, medium, and high charge density). For this purpose, nanoparticles which were used for these measurements were washed three times by centrifuging and redispersing them in Milli-Q water employing ultrasonic treatment (Table 3).
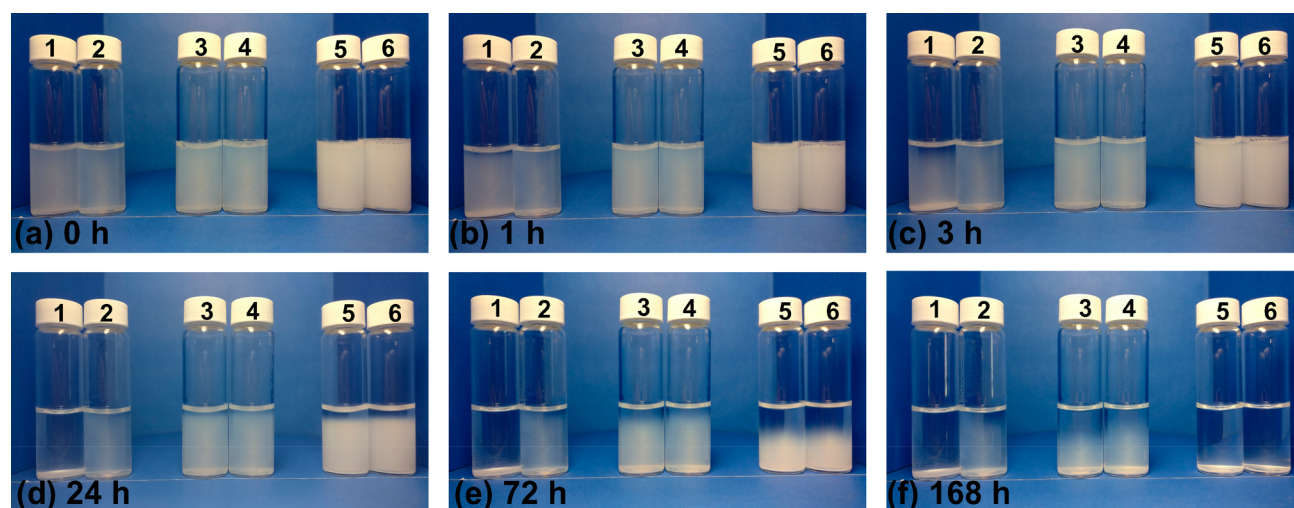
Figure 7. Visual evaluation of the aqueous dispersion stability (pH 6.5) of GdPO$_4$ particles with different morphologies ((nanorods (**1** bare, **2** modified), hexagonal nanoprisms (**3** bare, **4** modified), and submicrospheres (**5** bare, **6** modified)) over time: (a) 0, (b) 1, (c) 3, (d) 24, (e) 72, and (f) 168 h.

The results presented in Table 3 suggest that the equilibrium adsorption (independent of that of the used polymers) on GdPO$_4$ nanorods is higher in comparison to that of particles with other morphologies (hexagonal nanoprisms and submicrospheres). For example, the equilibrium adsorption of low-charge-density p(METAC-*stat*-PEO$_{19}$MEMA) on GdPO$_4$ nanorods is 39.2 mg/g if compared to 23.0 and 8.7 mg/g on hexagonal nanoprisms and submicrospheres, respectively. It can be explained through the particle size because it is well known that the surface area of particles is inversely proportional to the particle size, meaning that GdPO$_4$ nanorods are the smallest particles used in this study (Figure 1). To support this claim, nitrogen gas adsorption using the BET (Brunauer−Emmett−Teller) technique was conducted. During this analysis, the surface area was determined to be 47 m^2/g for nanorods, 24 m^2/g for hexagonal nanoprisms, and 20 m^2/g for submicrospheres.

Surface Potential and Colloidal Stability of Modified GdPO$_4$ Particles with Different Morphologies. Stable aqueous GdPO$_4$ particle dispersions (1 mg/mL) of each morphology were prepared by using dry GdPO$_4$ particles, which previously were washed and dried. The pH values of prepared GdPO$_4$ dispersions were then adjusted from ∼2 to 10.6 using 0.1 M HNO$_3$ and NH$_4$OH solutions, respectively. The zeta potential and particle size distribution were measured at different pH values for all GdPO$_4$ particle morphologies and are presented in Figure 6.

The IEPs of particles determined independently of the GdPO$_4$ particle morphology are shifted to the alkaline pH region. The p(METAC-*stat*-PEO$_{19}$MEMA) containing the largest number of charged groups (67 mol %) affected the IEP of the studied particles the most noticeably. For example, the IEPs of GdPO$_4$ nanorods modified with low- and medium-charge polymers were 7.23 and 8.65, respectively, whereas the IEP of nanorods stabilized with high-charge p(METAC-*stat*-PEO$_{19}$MEMA) was shifted to highly alkaline pH values (>11). The IEPs of GdPO$_4$ hexagonal nanoprisms were 6.99, 8.51, and ∼10.60 for particles modified using p(METAC-*stat*-PEO$_{19}$MEMA) with low, medium, and high charge densities, respectively. In the case of GdPO$_4$ submicrospheres, IEPs were determined to be 6.61, 7.96, and 8.98, respectively.

After GdPO$_4$ particle modification using cationic brush-type p(METAC-*stat*-PEO$_{19}$MEMA) polymers with different compositions, the stability range of GdPO$_4$ dispersions was expanded. It is important to notice that good stability is observed in the biological range (pH 6.6−7.4). The best results for the stabilization of GdPO$_4$ particles was achieved for rod-like particles. For comparison, bare GdPO$_4$ nanorods (IEP 6.53) were extremely unstable in the pH range from 4.2 to 9.1 (Figure 3b). Hence, after stabilization with polyelectrolytes, nanorods demonstrate perfect stability in the pH range from 2 up to 5.6, 7.2, and 8.3 using low-, medium- and high-charge polymers, respectively. The study of GdPO$_4$ particle stabilization with particles with other morphologies (hexagonal nanoprisms and submicrospheres) produced comparable results, which also suggest greatly increased colloidal stability (Figure 6).

The results obtained during this research imply that the most suitable investigated polymer for the stabilization of GdPO$_4$ particles tends to be the cationic brush-type p(METAC-*stat*-PEO$_{19}$MEMA) polyelectrolyte with the highest density of positively charged quaternary ammonium groups in its composition (65 mol %). The observed increase in GdPO$_4$ particle stability after surface modification was achieved as a combination of both steric and electrostatic stabilization because polymer-coated particles tend to possess positive surface charge, which provides additional electrostatic repulsion forces among modified particles. Therefore, this surface charge additionally enhances the particle stability.

Nanoparticles are often claimed to be potential candidates for biomedical (nanoprobes) and anticounterfeiting (security ink) applications. Low toxicity and good biocompatibility are highly desired properties for such nanoparticle systems, whereas superior colloidal stability is an absolute necessity.[60−63]

Long-Term Empirical Stability Experiment of Modified GdPO$_4$ Particles with Different Morphologies. One of the most remarkable results of this study is that after a relatively simple nanoparticle surface modification they can be easily redispersed from the dry powder and still form stable colloids. This, however, was not the case for the uncoated nanoparticles. Both nanoparticle preparation and their surface modification procedures are rather quick, easy, and simple and, most importantly, exhibit nearly perfect reproducibility, what is

crucial for scientific and commercial applications. It is also very important to notice that GdPO$_4$ particle surface modification using the p(METAC-*stat*-PEO$_{19}$MEMA) polyelectrolyte not only enhances the particle stability but also improves its biocompatibility.[64] Hence, we believe that the results achieved during this research may are important to the scientific community working in the field of nanoscience and colloid chemistry and could be applied in commercial applications.

In order to support our previous statement regarding nanoparticle stability and redispersibility, an additional experiment was planned and conducted. The main objective of this experiment was to evaluate the colloidal stability and redispersibility of both bare and modified nanoparticles. For this purpose, aqueous colloids (six colloids in total) were prepared using bare GdPO$_4$ nanoparticles with different morphologies (nanorods, hexagonal nanoprisms, and submicrospheres) and GdPO$_4$ particles (same morphology) modified with a high-charge-density (65 mol % quaternary ammonium groups) p(METAC-*stat*-PEO$_{19}$MEMA) polyelectrolyte. First, in order to evaluate the initial dispersibility, particles were redispersed from the dry state in neutral aqueous media (pH 6.5). It was noticed immediately that bare GdPO$_4$ nanorods, whose isoelectric point value is close to neutral pH values (Figure 3a), were redispersed considerably slower than GdPO$_4$ nanorods with modified surfaces. This observation was documented and can clearly be seen in a video (SI video). In a vial on the left-hand side there are bare GdPO$_4$ nanorods that were dried, whereas in a vial on the right-hand side there are the same GdPO$_4$ nanorods whose surfaces were modified with the polyelectrolyte. After the shaking of both vials, the bare GdPO$_4$ nanorods precipitate readily, while the surface-modified particles are disperses into the water and remain stable.

Another experiment involved the observation of GdPO$_4$ colloidal suspension stability in a time frame of up to 168 h (1 week). For this purpose, aqueous colloids of GdPO$_4$ particles (both bare and modified) with different morphologies were prepared and documented over the given time. Visual colloidal stability over time is represented in Figure 7. All samples were redispersed by treating the colloids in an ultrasonic bath for 5 min.

It is important to notice that differently shaped GdPO$_4$ nanoparticles possess different zeta potential values at the same pH value. This means that in the same aqueous media (for example, during this experiment) they also have to have different zeta-potential values. This is because the isoelectric point (and therefore the zeta potential value) is dependent on the particle morphology, as discussed above. During this experiment (in which the pH of aqueous media was set to 6.5), zeta potential values of bare GdPO$_4$ nanoparticles were +0.56, −9.0, and −18.6 mV for nanorods, hexagonal nanoprisms, and submicrospheres, respectively. Meanwhile, identical aqueous colloids (pH 6.5) were prepared by dispersing GdPO$_4$ particles modified with the high-charge-density p(METAC-*stat*-PEO$_{19}$MEMA) polyelectrolyte. Zeta potential values of such colloids were ca. +22 mV for all morphologies identical to those presented in Figure 6a−c. Because modified GdPO$_4$ particles of all morphologies have almost identical zeta potential values, it is possible to additionally evaluate the effectiveness of cationic brush-type polymers as a function of the shape of the modified particles. It is known that due to the electrostatic repulsion forces even insignificant nanoparticle surface charge could affect the overall stability of such particle colloids. Therefore, according to Figure 3b, bare GdPO$_4$ hexagonal nanoprisms

and submicrospheres should exhibit better colloidal stability during this experiment in comparison to bare GdPO$_4$ nanorods.

No obvious visual difference between colloids of the same morphology was observed after ultrasonically redispersing both bare and modified GdPO$_4$ particles of various morphologies in aqueous media (pH 6.5) (Figure 7a). However, it should be noticed that the aqueous colloid of bare GdPO$_4$ nanorods (Figure 7a, **1**) was slightly hazier in comparison to the colloid obtained by redispersing modified GdPO$_4$ nanorods (Figure 7a, **2**). After 1 h (Figure 7b), a transparent layer developed and is observed in the upper part of the bare GdPO$_4$ nanorod colloids (Figure 7b, **1**). This indicates the sedimentation of bare GdPO$_4$ nanorods. This transparent layer broadens over time and becomes more highly expressed in images taken after 3 h (Figure 7c, **1**). In the case of GdPO$_4$ nanoprisms (**3** and **4**) and submicrospheres (**5** and **6**), no obvious differences between bare and modified aqueous colloids were observed in the time frame of up to 3 h (Figure 7c). Twenty-four hours after the beginning of the experiment, the sedimentation of bare GdPO$_4$ nanorods (Figure 7d, **1**) becomes even more evident, while modified GdPO$_4$ nanorod colloids show no signs of sedimentation (Figure 7d, **2**). Controversially, dispersions of both bare and modified GdPO$_4$ hexagonal nanoprisms (**3** and **4**) even after 24 h remain in the state of stable aqueous colloids (Figure 7d, **3** and **4**). Slight settling is observed for both bare and modified GdPO$_4$ submicrospheres (Figure 7d, **5** and **6**). Visual observations 72 h after the beginning of the experiment revealed that bare GdPO$_4$ nanorods have completely precipitated, whereas modified GdPO$_4$ nanorod colloids remained stable. Both bare and modified hexagonal nanoprism colloids show signs of sedimentation after 72 h of experiment, though modified prism settling is less expressed in comparison with that of bare prisms (Figure 7e, **3** and **4**). Regardless of modified or bare, particle-weight-related settling of submicrospheres continues 72 h after the start of the experiment (Figure 7e, **5** and **6**). By the end of the experiment (after 168 h), bare GdPO$_4$ nanorods (Figure 7f, **1**) were completely precipitated, whereas modified GdPO$_4$ nanorods were only slightly settled (Figure 7f, **2**) but were still in the state of stable aqueous colloids. Also, a more rapid sedimentation of bare hexagonal nanoprisms (Figure 7f, **3**) becomes more noticeable over time because after 168 h bare prisms were clearly more settled if compared to modified hexagonal nanoprisms (Figure 7f, **4**). The difference in the colloidal stability of bare and modified hexagonal nanoprisms could indicate the possible agglomeration of bare hexagonal nanoprisms. Both bare and modified GdPO$_4$ submicrospheres completely precipitated after 168 h (Figure 7f, **5** and Figure 7f, **6**). The reason for such sedimentation of submicrospheres could probably be related to the relatively large mass and dimensions (>100 nm) of GdPO$_4$ submicrospheres (if compared to those of GdPO$_4$ nanorods and hexagonal nanoprisms). We emphasize that it is not accurate to evaluate particle agglomeration only by judging the visually observed sedimentation of particles. Zeta potential values of both bare and modified submicrospheres in observed colloids are rather high (i.e., −18.6 and +22.7 mV, respectively). Such zeta potential values should be high enough to induce a strong enough electrostatic repulsion force to prevent submicrosphere agglomeration. So to conclude, this sedimentation is likely to be caused by gravity accompanied by the relatively large weight of GdPO$_4$ submicrospheres.

Until this moment, colloidal stability during this experiment was evaluated only visually. However, such an approach does not really tell us anything about the real scale of particle
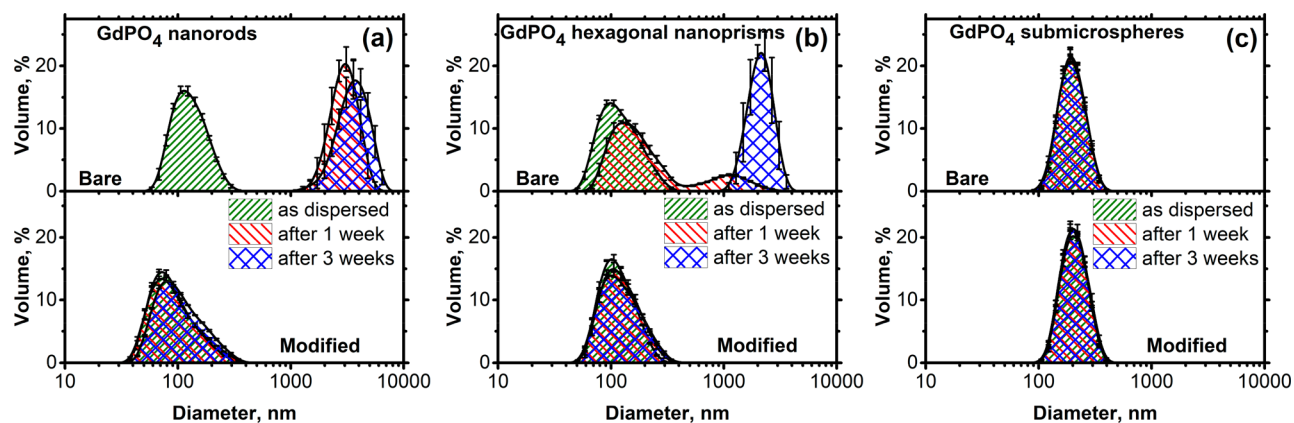
Figure 8. Particle size distribution in aqueous dispersions (pH 6.5) of GdPO$_4$ particles with different morphologies after different periods of storage (as dispersed, after 1 week and after 3 weeks): (a) nanorods, (b) hexagonal nanoprisms, and (c) submicrospheres.

agglomeration. In order to justify our claims and hypotheses derived from visual observations of GdPO$_4$ colloids during this experiment, dynamic light scattering measurements were conducted. After the visual experiment ended (colloids withstood 168 h), aqueous dispersions were prepared for DLS measurements by simply shaking GdPO$_4$ colloids for 20−30 s (no ultrasonic treatment was used). After that, DLS measurements were performed and the particle size distribution was determined (Figure 8). Additional DLS measurements were conducted again 3 weeks after the initial redispersion of particles.

DLS measurements revealed that after 168 h (1 week) bare GdPO$_4$ nanorods were in an agglomerated state (Figure 8a) with an agglomerate size varying around 2700 nm. Additional DLS measurements after 504 h (3 weeks) indicated the further agglomeration of bare GdPO$_4$ nanorods (Figure 8a), with the agglomerate size increasing up to around 3600 nm. Such a result was expected as bare GdPO$_4$ nanorods are close to their isoelectric point (ζ = +0.56 mV) in neutral media (pH 6.5). These particles are completely unstable and therefore are inapplicable in all intended applications. According to the DLS measurements, GdPO$_4$ nanorods modified with p(METAC-*stat*-PEO$_{19}$MEMA) cationic brush polyelectrolytes are perfectly stable, with a size of around 70 nm even after 3 weeks of storage. Contrary to bare GdPO$_4$ nanorods, GdPO$_4$ hexagonal nanoprisms have a slightly expressed negative zeta potential value of −9.0 mV at a pH value of 6.5. Such a zeta potential value is enough to inhibit the agglomeration of particles but not enough to ensure the overall colloidal stability of GdPO$_4$ hexagonal nanoprisms over extended periods of time. Complete agglomeration of bare GdPO$_4$ hexagonal nanoprisms, with the agglomerate size varying around 2300 nm, was observed 3 weeks after the initial redispersion (Figure 8b). Therefore, under the given conditions, hexagonal nanoprisms are more stable if compared to rod-like GdPO$_4$ nanoparticles, but their colloidal stability is still far from superior. PSD curves, obtained by volume means of DLS, show a bimodal distribution in aqueous colloids of bare GdPO$_4$ hexagonal nanoprisms after 1 week (Figure 8b). One peak representing particles of around 105 nm in size can be attributed to stable particles, and other peaks represent hexagonal nanoprism agglomerates of around 1100 nm in size. The PSD curve of bare hexagonal nanoprisms indicates complete agglomeration 3 weeks after the initial redispersion, with the agglomerate size varying around 2300 nm (Figure 8b). As expected, PSD curves of modified GdPO$_4$

nanoprisms (Figure 8b) show a monomodal distribution, indicating that no agglomeration processes occurred during the 3 weeks of the experiment.

Further DLS measurements revealed that even after 1 week of observation both bare and modified GdPO$_4$ submicrospheres were completely settled due to the relatively large values of the zeta potential (−18.6 and +22.7 mV for bare and modified particles, respectively), and these particles show no agglomeration. As seen in Figure 8c, PSD is monomodal with its maximum value at around 180 nm. DLS measurements indicated that no signs of agglomeration were observed even 3 weeks after the initial redispersion. Such results confirmed our hypothesis that the sedimentation of submicrospheres was induced only by a relatively large particle weight.

This work leads to the conclusion that the visual evaluation of nanoparticle colloidal stability, which is very typical in many papers, is not sufficient. Such visual stability evaluation in scientific papers and research is inappropriate and could even be referred to as incorrect. Indeed, if evaluated particles are observably unstable, as it was with bare GdPO$_4$ nanorods in our case, then it can be concluded that aqueous colloids are unstable, even though it takes time for visual sedimentation to occur. Meanwhile, if particles have relatively large surface charge (as with GdPO$_4$ submicrospheres in this work) but they sediment over time as well (as discussed above, the sedimentation of stable GdPO$_4$ submicrospheres occurred due to particle weight), then they can be wrongly considered to be agglomerates. Therefore, we strongly suggest that the colloidal stability of aqueous dispersions should be confirmed not only visually but also by means of light-scattering measurements (either dynamic or static).

Stability of GdPO$_4$ Particles in Biological Aqueous Media. One of the most remarkable features of this study is that the described concept of particle stabilization could be successfully applied in biological media. To prove this statement, an additional experiment was carried out by dispersing both bare and modified GdPO$_4$ in protein-rich aqueous media (consisting of 10 vol % human blood plasma, pH 6.5). First, particle dispersions were observed visually. It was noticed that bare particles, regardless their morphology (nanorods, hexagonal nanoprisms, or submicrospheres), have a greater tendency to sediment compared to modified particles. The visual stability observations are presented in Figure S4. The dry GdPO$_4$ powders (both bare and modified) were dispersed in protein-rich aqueous media and incubated for 3 h. Then the dispersion

was centrifuged (10 000 rpm for 15 min) and particles were washed with DI water (procedure repeated three times) to remove the excess proteins. Washed particles were redispersed in water (pH 6.5), and the PSD of nanoparticle−protein conjugates was measured via DLS (Figure S5). The protein antifouling properties of modified particles were also evaluated by comparing the change in the zeta potential of particles incubated in protein-rich media with those dispersed in protein-free aqueous media (pH 6.5). The obtained results are presented in Figure 9.
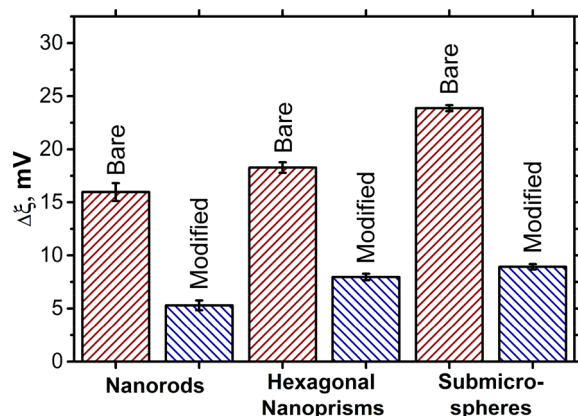
Figure 9. Change in the zeta potential of particles in protein-rich aqueous media (consisting of 10 vol % human blood plasma) compared to those dispersed in protein-free aqueous media (pH 6.5).

The smaller change in the zeta potential of modified GdPO$_4$ particles (more than twice regardless of the particle morphology) indicates that a smaller amount of proteins is adsorbed by (surrounds) the particles. Significant differences in the zeta potential change prove that PEG substituents existing on the surfaces of modified GdPO$_4$ particles provide antifouling properties and significantly reduce protein binding. Therefore, these results are in perfect correlation with the results obtained by measuring the PSD, where modified particle−polymer conjugates exhibited a smaller size if compared to bare particle−protein ones, which were nonstable and sedimented rapidly (Figure S5).

CONCLUSIONS

Cationic brush-type polyelectrolytes p(METAC-*stat*-PEO$_{19}$MEMA) with three different compositions were synthesized and applied with the aim of stabilizing aqueous dispersions of bare GdPO$_4$ particles (nanorods, hexagonal nanoprisms, and submicrospheres). Colloidal stability and zeta potential studies of bare GdPO$_4$ particles revealed that exhibited IEP values of GdPO$_4$ particles are dependent on their morphology and are 6.53, 6.03, and 5.61, for nanorods, hexagonal nanoprisms, and submicrospheres, respectively. Regardless of their morphology, particles had typical unstable zones if the absolute zeta potential is lower than |22| mV. Cationic brush-type p(METAC-*stat*-PEO$_{19}$MEMA) copolymers had a significant effect on the surface potential and overall stability of GdPO$_4$ particles. Apparently, the p(METAC-*stat*-PEO$_{19}$MEMA) polyelectrolytes with the largest number of charged groups (65 mol %) have the largest impact on the surface charge of GdPO$_4$ particles. During titrations using such polymers, the charge inversion effect was observed independently of the morphology of GdPO$_4$ particles used. The stability and zeta potential of modified GdPO$_4$ particle

dispersions at different pH values were evaluated. The unstable zones of surface-modified GdPO$_4$ particles were narrowed, and the determined isoelectric point values were shifted to the alkaline region if compared to the bare particles. Highly charged p(METAC-*stat*-PEO$_{19}$MEMA) brush polyelectrolytes used to modify the surfaces of GdPO$_4$ particles enabled superior particle stability in the biological pH range, which could extend the applicability of such unique particles in the biotechnology field. Long-term stability measurements (DLS) indicated a monomodal PSD for all investigated modified GdPO$_4$ nanoparticles with no signs of agglomeration after 3 weeks from the initial redispersion. In the case of bare GdPO$_4$ nanoparticles, complete agglomeration is observed. The stability experiment in protein-rich aqueous media (consisting of 10 vol % human blood plasma) showed that PEG substituents on the surface of modified GdPO$_4$ particles provide antifouling properties that significantly reduce the formation of particle−protein conjugates.

We also point out that the most remarkable feature of the nanoparticle modification with the brush-type polyelectrolytes during this research is that such modified nanoparticles can be dried and later easily redispersed without any negative effects on the colloid stability. This approach has huge advantages in both scientific and commercial fields. For the former, it is much easier to prepare the desired nanoparticle concentration from the powder, whereas for the latter the handling, storage, and shipping of dry powders instead of diluted colloids are also much easier and more cost-effective. Moreover, particles whose surfaces are modified/covered with polymers containing PEO substituents tend to have reduced toxicity and improved biocompatibility.

ASSOCIATED CONTENT

ⓢ Supporting Information

The Supporting Information is available free of charge at https://pubs.acs.org/doi/10.1021/acs.langmuir.0c01130.

> Detailed GdPO$_4$ particle synthesis procedure; XRD patterns and SEC measurements; ^{1}H NMR spectra; and GdPO$_4$ particle stability in biological media: visual experiment and PSD curves (PDF)

> Slow redispersion of bare GdPO$_4$ nanorods compared to that of GdPO$_4$ nanorods with a modified surface (MP4)

AUTHOR INFORMATION

Corresponding Author

> **Arturas Katelnikovas** − *Institute of Chemistry, Vilnius University, LT-03225 Vilnius, Lithuania;* ⓞ orcid.org/0000-0002-3295-8366; Email: arturas.katelnikovas@chf.vu.lt

Authors

> **Vaidas Klimkevicius** − *Institute of Chemistry, Vilnius University, LT-03225 Vilnius, Lithuania*
> **Matas Janulevicius** − *Institute of Chemistry, Vilnius University, LT-03225 Vilnius, Lithuania*
> **Aleksandra Babiceva** − *Institute of Chemistry, Vilnius University, LT-03225 Vilnius, Lithuania*
> **Audrius Drabavicius** − *Centre of Physical Science and Technology, LT-10257 Vilnius, Lithuania*

Complete contact information is available at:
https://pubs.acs.org/10.1021/acs.langmuir.0c01130

■ REFERENCES

(1) Talapin, D. V.; Shevchenko, E. V. Introduction: Nanoparticle Chemistry. *Chem. Rev.* **2016**, *116* (18), 10343−10345.

(2) Uglov, V. V.; Doroshevich, I. L.; Kvasov, N. T.; Remnev, G. E.; Shymanski, V. I. On Physical Properties of Nanoparticles: Size Effect and Scale of Nanoobjects. *Phys. status solidi c* **2016**, *13* (10−12), 903−907.

(3) Jeevanandam, J.; Barhoum, A.; Chan, Y. S.; Dufresne, A.; Danquah, M. K. Review on Nanoparticles and Nanostructured Materials: History, Sources, Toxicity and Regulations. *Beilstein J. Nanotechnol.* **2018**, *9*, 1050−1074.

(4) Mourdikoudis, S.; Pallares, R. M.; Thanh, N. T. K. Characterization Techniques for Nanoparticles: Comparison and Complementarity upon Studying Nanoparticle Properties. *Nanoscale* **2018**, *10* (27), 12871−12934.

(5) Teo, R. D.; Termini, J.; Gray, H. B. Lanthanides: Applications in Cancer Diagnosis and Therapy. *J. Med. Chem.* **2016**, *59* (13), 6012−6024.

(6) Björnmalm, M.; Thurecht, K. J.; Michael, M.; Scott, A. M.; Caruso, F. Bridging Bio-Nano Science and Cancer Nanomedicine. *ACS Nano* **2017**, *11* (10), 9594−9613.

(7) Cassano, D.; Pocoví-Martínez, S.; Voliani, V. Ultrasmall-in-Nano Approach: Enabling the Translation of Metal Nanomaterials to Clinics. *Bioconjugate Chem.* **2018**, *29* (1), 4−16.

(8) Levchenko, I.; Xu, S.; Teel, G.; Mariotti, D.; Walker, M. L. R.; Keidar, M. Recent Progress and Perspectives of Space Electric Propulsion Systems Based on Smart Nanomaterials. *Nat. Commun.* **2018**, *9* (1), 879.

(9) Giraldo, J. P.; Wu, H.; Newkirk, G. M.; Kruss, S. Nanobiotechnology Approaches for Engineering Smart Plant Sensors. *Nat. Nanotechnol.* **2019**, *14* (6), 541−553.

(10) Graf, C.; Gao, Q.; Schütz, I.; Noufele, C. N.; Ruan, W.; Posselt, U.; Korotianskiy, E.; Nordmeyer, D.; Rancan, F.; Hadam, S.; Vogt, A.; Lademann, J.; Haucke, V.; Rühl, E. Surface Functionalization of Silica Nanoparticles Supports Colloidal Stability in Physiological Media and Facilitates Internalization in Cells. *Langmuir* **2012**, *28* (20), 7598−7613.

(11) Fang, C.; Bhattarai, N.; Sun, C.; Zhang, M. Functionalized Nanoparticles with Long-Term Stability in Biological Media. *Small* **2009**, *5* (14), 1637−1641.

(12) Marins, J. A.; Montagnon, T.; Ezzaier, H.; Hurel, C.; Sandre, O.; Baltrunas, D.; Mazeika, K.; Petrov, A.; Kuzhir, P. Colloidal Stability of Aqueous Suspensions of Polymer-Coated Iron Oxide Nanorods: Implications for Biomedical Applications. *ACS Appl. Nano Mater.* **2018**, *1* (12), 6760−6772.

(13) Doblas, D.; Kister, T.; Cano-Bonilla, M.; González-García, L.; Kraus, T. Colloidal Solubility and Agglomeration of Apolar Nanoparticles in Different Solvents. *Nano Lett.* **2019**, *19* (8), 5246−5252.

(14) Phan, H. T.; Haes, A. J. What Does Nanoparticle Stability Mean? *J. Phys. Chem. C* **2019**, *123* (27), 16495−16507.

(15) Zhong, C.; Yang, P.; Li, X.; Li, C.; Wang, D.; Gai, S.; Lin, J. Monodisperse Bifunctional Fe_3O_4@$NaGdF_4$:Yb/Er@$NaGdF_4$: Yb/Er Core-Shell Nanoparticles. *RSC Adv.* **2012**, *2* (8), 3194−3197.

(16) Tian, J.; Zhang, F.; Han, Y.; Zhao, X.; Chen, C.; Zhang, C.; Jia, G. Template-Directed Synthesis, Properties, and Dual-Modal Bioapplica-

tions of Multifunctional $GdPO_4$ Hierarchical Hollow Spheres. *Appl. Surf. Sci.* **2019**, *475*, 264−272.

(17) Zhu, G.; Chen, L.; Zeng, F.; Gu, L.; Yu, X.; Li, X.; Jiang, J.; Guo, G.; Cao, J.; Tang, K.; Zhu, H.; Daldrup-Link, H. E.; Wu, M. $GdVO_4$:Eu^{3+}, Bi^{3+} Nanoparticles as a Contrast Agent for MRI and Luminescence Bioimaging. *ACS Omega* **2019**, *4* (14), 15806−15814.

(18) Kuang, X.; Liu, H.; Hu, W.; Shao, Y. Hydrothermal Synthesis of Core-Shell Structured $TbPO_4$:Ce^{3+}@$TbPO_4$:Gd^{3+} Nanocomposites for Magnetic Resonance and Optical Imaging. *Dalt. Trans.* **2014**, *43* (32), 12321−12328.

(19) Gai, S.; Li, C.; Yang, P.; Lin, J. Recent Progress in Rare Earth Micro/Nanocrystals: Soft Chemical Synthesis, Luminescent Properties, and Biomedical Applications. *Chem. Rev.* **2014**, *114* (4), 2343−2389.

(20) Bouzigues, C.; Gacoin, T.; Alexandrou, A. Biological Applications of Rare-Earth Based Nanoparticles. *ACS Nano* **2011**, *5* (11), 8488−8505.

(21) Cao, Y.; Xu, L.; Kuang, Y.; Xiong, D.; Pei, R. Gadolinium-Based Nanoscale MRI Contrast Agents for Tumor Imaging. *J. Mater. Chem. B* **2017**, *5* (19), 3431−3461.

(22) Jeong, Y.; Hwang, H. S.; Na, K. Theranostics and Contrast Agents for Magnetic Resonance Imaging. *Biomater. Res.* **2018**, *22*, 20.

(23) Xu, J.; Shen, X.; Jia, L.; Ge, Z.; Zhou, D.; Yang, Y.; Ma, T.; Luo, Y.; Zhu, T. $GdPO_4$-Based Nanoprobe for Bioimaging and Selective Recognition of Dipicolinic Acid and Cysteine by a Sensing Ensemble Approach. *ACS Biomater. Sci. Eng.* **2019**, *5* (2), 996−1004.

(24) Yan, Z.-G.; Yan, C.-H. Controlled Synthesis of Rare Earth Nanostructures. *J. Mater. Chem.* **2008**, *18* (42), 5046−5059.

(25) Yin, S.; Akita, S.; Shinozaki, M.; Li, R.; Sato, T. Synthesis and Morphological Control of Rare Earth Oxide Nanoparticles by Solvothermal Reaction. *J. Mater. Sci.* **2008**, *43* (7), 2234−2239.

(26) Rostami, I.; Rezvani Alanagh, H.; Hu, Z.; Shahmoradian, S. H. Breakthroughs in Medicine and Bioimaging with Up-Conversion Nanoparticles. *Int. J. Nanomed.* **2019**, *14*, 7759−7780.

(27) Wen, S.; Zhou, J.; Zheng, K.; Bednarkiewicz, A.; Liu, X.; Jin, D. Advances in Highly Doped Upconversion Nanoparticles. *Nat. Commun.* **2018**, *9* (1), 2415.

(28) Smith, B. R.; Gambhir, S. S. Nanomaterials for In Vivo Imaging. *Chem. Rev.* **2017**, *117* (3), 901−986.

(29) Cao, P.; Tong, L.; Hou, Y.; Zhao, G.; Guerin, G.; Winnik, M. A.; Nitz, M. Improving Lanthanide Nanocrystal Colloidal Stability in Competitive Aqueous Buffer Solutions Using Multivalent PEG-Phosphonate Ligands. *Langmuir* **2012**, *28* (35), 12861−12870.

(30) Boyer, J.-C.; Cuccia, L. A.; Capobianco, J. A. Synthesis of Colloidal Upconverting $NaYF_4$: Er^{3+}/Yb^{3+} and Tm^{3+}/Yb^{3+} Monodisperse Nanocrystals. *Nano Lett.* **2007**, *7* (3), 847−852.

(31) Abel, K. A.; Boyer, J.-C.; Veggel, F. C. J. M. van. Hard Proof of the $NaYF_4$/$NaGdF_4$ Nanocrystal Core/Shell Structure. *J. Am. Chem. Soc.* **2009**, *131* (41), 14644−14645.

(32) Liang, S.; Zhang, X.; Wu, Z.; Liu, Y.; Zhang, H.; Sun, H.; Sun, H.; Yang, B. Decoration of Up-Converting $NaYF_4$:Yb, Er(Tm) Nanoparticles with Surfactant Bilayer. A Versatile Strategy to Perform Oil-to-Water Phase Transfer and Subsequently Surface Silication. *CrystEngComm* **2012**, *14* (10), 3484−3489.

(33) Sedlmeier, A.; Gorris, H. H. Surface Modification and Characterization of Photon-Upconverting Nanoparticles for Bioanalytical Applications. *Chem. Soc. Rev.* **2015**, *44* (6), 1526−1560.

(34) Becerro, A. I.; Rodríguez-Liviano, S.; Fernández-Carrión, A. J.; Ocaña, M. A Novel 3D Architecture of $GdPO_4$ Nanophosphors: Multicolored and White Light Emission. *Cryst. Growth Des.* **2013**, *13* (2), 526−535.

(35) Achary, S. N.; Bevara, S.; Tyagi, A. K. Recent Progress on Synthesis and Structural Aspects of Rare-Earth Phosphates. *Coord. Chem. Rev.* **2017**, *340*, 266−297.

(36) Lai, H.; Bao, A.; Yang, Y.; Tao, Y.; Yang, H. Selective Synthesis and Luminescence Property of Monazite- and Hexagonal-Type $LaPO_4$:Eu Nanocrystals. *CrystEngComm* **2009**, *11* (6), 1109−1113.

(37) Patra, C. R.; Alexandra, G.; Patra, S.; Jacob, D. S.; Gedanken, A.; Landau, A.; Gofer, Y. Microwave Approach for the Synthesis of

Rhabdophane-Type Lanthanide Orthophosphate (Ln = La, Ce, Nd, Sm, Eu, Gd and Tb) Nanorods under Solvothermal Conditions. *New J. Chem.* **2005**, *29* (5), 733−739.

(38) Tsuda, A.; Venkata, N. K. The Role of Natural Processes and Surface Energy of Inhaled Engineered Nanoparticles on Aggregation and Corona Formation. *Nano Impact* **2016**, *2*, 38−44.

(39) Hifumi, H.; Yamaoka, S.; Tanimoto, A.; Citterio, D.; Suzuki, K. Gadolinium-Based Hybrid Nanoparticles as a Positive MR Contrast Agent. *J. Am. Chem. Soc.* **2006**, *128* (47), 15090−15091.

(40) Sahu, N. K.; Shanta Singh, N.; Ningthoujam, R. S.; Bahadur, D. Ce^{3+}-Sensitized $GdPO_4$:Tb^{3+} Nanorods: An Investigation on Energy Transfer, Luminescence Switching, and Quantum Yield. *ACS Photonics* **2014**, *1* (4), 337−346.

(41) Ren, W.; Tian, G.; Zhou, L.; Yin, W.; Yan, L.; Jin, S.; Zu, Y.; Li, S.; Gu, Z.; Zhao, Y. Lanthanide Ion-Doped $GdPO_4$ Nanorods with Dual-Modal Bio-Optical and Magnetic Resonance Imaging Properties. *Nanoscale* **2012**, *4* (12), 3754−3760.

(42) Yan, R.; Sun, X.; Wang, X.; Peng, Q.; Li, Y. Crystal Structures, Anisotropic Growth, and Optical Properties: Controlled Synthesis of Lanthanide Orthophosphate One-Dimensional Nanomaterials. *Chem. - Eur. J.* **2005**, *11* (7), 2183−2195.

(43) Yi, Z.; Lu, W.; Qian, C.; Zeng, T.; Yin, L.; Wang, H.; Rao, L.; Liu, H.; Zeng, S. Urchin-like Ce/Tb Co-Doped $GdPO_4$ Hollow Spheres for in Vivo Luminescence/X-Ray Bioimaging and Drug Delivery. *Biomater. Sci.* **2014**, *2* (10), 1404−1411.

(44) Xu, Z.; Cao, Y.; Li, C.; Ma, P.; Zhai, X.; Huang, S.; Kang, X.; Shang, M.; Yang, D.; Dai, Y.; Lin, J. Urchin-like $GdPO_4$ and $GdPO_4$:Eu^{3+} Hollow Spheres - Hydrothermal Synthesis, Luminescence and Drug-Delivery Properties. *J. Mater. Chem.* **2011**, *21* (11), 3686−3694.

(45) Rodriguez-Liviano, S.; Becerro, A. I.; Alcántara, D.; Grazú, V.; de la Fuente, J. M.; Ocaña, M. Synthesis and Properties of Multifunctional Tetragonal Eu:$GdPO_4$ Nanocubes for Optical and Magnetic Resonance Imaging Applications. *Inorg. Chem.* **2013**, *52* (2), 647−654.

(46) Janulevicius, M.; Klimkevicius, V.; Vanetsev, A.; Plausinaitiene, V.; Sakirzanovas, S.; Katelnikovas, A. Controlled Hydrothermal Synthesis, Morphological Design and Colloidal Stability of $GdPO_4$·nH2O Particles. *Mater. Today Commun.* **2020**, *23*, 100934.

(47) Singh, K.; Raghav, A.; Jha, P. K.; Satapathi, S. Effect of Size and Charge Asymmetry on Aggregation Kinetics of Oppositely Charged Nanoparticles. *Sci. Rep.* **2019**, *9* (1), 3762.

(48) Mohrhusen, L.; Osmić, M. Sterical Ligand Stabilization of Nanocrystals versus Electrostatic Shielding by Ionic Compounds: A Principle Model Study with TEM and XPS. *RSC Adv.* **2017**, *7* (21), 12897−12907.

(49) Moore, T. L.; Rodriguez-Lorenzo, L.; Hirsch, V.; Balog, S.; Urban, D.; Jud, C.; Rothen-Rutishauser, B.; Lattuada, M.; Petri-Fink, A. Nanoparticle Colloidal Stability in Cell Culture Media and Impact on Cellular Interactions. *Chem. Soc. Rev.* **2015**, *44* (17), 6287−6305.

(50) Heijman, S. G. J.; Stein, H. N. Electrostatic and Sterical Stabilization of TiO_2 Dispersions. *Langmuir* **1995**, *11* (2), 422−427.

(51) Klimkevicius, V.; Graule, T.; Makuska, R. Effect of Structure of Cationic Comb Copolymers on Their Adsorption and Stabilization of Titania Nanoparticles. *Langmuir* **2015**, *31* (7), 2074−2083.

(52) Yang, J.; Deng, Y.; Wu, Q.; Zhou, J.; Bao, H.; Li, Q.; Zhang, F.; Li, F.; Tu, B.; Zhao, D. Mesoporous Silica Encapsulating Upconversion Luminescence Rare-Earth Fluoride Nanorods for Secondary Excitation. *Langmuir* **2010**, *26* (11), 8850−8856.

(53) Heuer-Jungemann, A.; Feliu, N.; Bakaimi, I.; Hamaly, M.; Alkilany, A.; Chakraborty, I.; Masood, A.; Casula, M. F.; Kostopoulou, A.; Oh, E.; Susumu, K.; Stewart, M. H.; Medintz, I. L.; Stratakis, E.; Parak, W. J.; Kanaras, A. G. The Role of Ligands in the Chemical Synthesis and Applications of Inorganic Nanoparticles. *Chem. Rev.* **2019**, *119* (8), 4819−4880.

(54) Ramos Guivar, J. A.; Sanches, E. A.; Magon, C. J.; Ramos Fernandes, E. G. Preparation and Characterization of Cetyltrimethylammonium Bromide (CTAB)-Stabilized Fe_3O_4 Nanoparticles for Electrochemistry Detection of Citric Acid. *J. Electroanal. Chem.* **2015**, *755*, 158−166.

(55) Baziulyte-Paulaviciene, D.; Traskina, N.; Vargalis, R.; Katelnikovas, A.; Sakirzanovas, S. Thermal Decomposition Synthesis of Er^{3+}-Activated $NaYbF_4$ Upconverting Microparticles for Optical Temperature Sensing. *J. Lumin.* **2019**, *215*, 116672.

(56) Ran, Q.; Qiao, M.; Liu, J.; Miao, C. SMA-g-MPEG Comb-like Polymer as a Dispersant for Al_2O_3 Suspensions. *Appl. Surf. Sci.* **2012**, *258* (7), 2447−2453.

(57) Rhodes, S. K.; Lambeth, R. H.; Gonzales, J.; Moore, J. S.; Lewis, J. A. Cationic Comb Polymer Superdispersants for Colloidal Silica Suspensions. *Langmuir* **2009**, *25* (12), 6787−6792.

(58) Klimkevicius, V.; Steponaviciute, M.; Makuska, R. Kinetics of RAFT Polymerization and Copolymerization of Vinyl Monomers by Size Exclusion Chromatography. *Eur. Polym. J.* **2020**, *122*, 109356.

(59) Karimi, Z.; Karimi, L.; Shokrollahi, H. Nano-Magnetic Particles Used in Biomedicine: Core and Coating Materials. *Mater. Sci. Eng., C* **2013**, *33* (5), 2465−2475.

(60) Albanese, A.; Chan, W. C. W. Effect of Gold Nanoparticle Aggregation on Cell Uptake and Toxicity. *ACS Nano* **2011**, *5* (7), 5478−5489.

(61) Wu, J.; Zhang, X.; Yao, T.; Li, J.; Zhang, H.; Yang, B. Improvement of the Stability of Colloidal Gold Superparticles by Polypyrrole Modification. *Langmuir* **2010**, *26* (11), 8751−8755.

(62) Sugumaran, P. J.; Liu, X.-L.; Herng, T. S.; Peng, E.; Ding, J. GO-Functionalized Large Magnetic Iron Oxide Nanoparticles with Enhanced Colloidal Stability and Hyperthermia Performance. *ACS Appl. Mater. Interfaces* **2019**, *11* (25), 22703−22713.

(63) Rivera Gil, P.; Oberdörster, G.; Elder, A.; Puntes, V.; Parak, W. J. Correlating Physico-Chemical with Toxicological Properties of Nanoparticles: The Present and the Future. *ACS Nano* **2010**, *4* (10), 5527−5531.

(64) Suk, J. S.; Xu, Q.; Kim, N.; Hanes, J.; Ensign, L. M. PEGylation as a Strategy for Improving Nanoparticle-Based Drug and Gene Delivery. *Adv. Drug Delivery Rev.* **2016**, *99* (Pt A), 28−51.

Supporting information

Effect of Cationic Brush-Type Copolymers on Colloidal Stability of GdPO$_4$ Particles with Different Morphology in Biological Aqueous Media

Vaidas Klimkevicius[1, ‡], Matas Janulevicius[1, ‡], Aleksandra Babiceva[1], Audrius Drabavicius[2] and Arturas Katelnikovas[1,*]

[1] Institute of Chemistry, Vilnius University, Naugarduko 24, LT-03225 Vilnius, Lithuania.

[2] Centre of Physical Science and Technology, Sauletekis av. 3, LT-10257 Vilnius, Lithuania.

Email: arturas.katelnikovas@chf.vu.lt

Number of pages: 8
Number of figures: 5

Content

S1. Instrumental analysis methods

S1.1. Size exclusion chromatography (SEC) measurements. The macromolecular parameters of the synthesized p(METAC-*stat*-PEO$_{19}$MEMA) copolymers such as number average and weight average molecular weights (M_n and M_w), and dispersity ($Đ = M_w/M_n$) were determined by size exclusion chromatography (SEC). Viscotek TDAmax (Malvern) system equipped with a triple detection array (TDA305) consisting of a differential refractive index detector (RI), light scattering detector (LS) simultaneously measuring the scattered light (laser 3 mW, 670 nm) at two angles – right-angle (90°) and low-angle (7°), and four-capillary bridge viscosity detector (IV) was used. Viscotek (Malvern) columns AGuard (50 × 8.0 mm) and A6000M General Mixed Aq (300 × 8.0 mm) filled with porous polyhydroxymethacrylate, particle size 13 μm, nominal pore size $1.5 × 10^4$ Å, exclusion limit M_w (for Pollulan) < $2·10^7$ g/mol, were employed for the separation of hydrophilic polymeric samples. A 250 mM sodium acetate buffer (pH 4.0) was used as an eluent, flow rate was 0.5 mL/min. The temperature of the column oven and of the detectors was maintained at 30.0 °C. The prepared diluted polymer samples with concentration of 2-4 mg/mL were injected into SEC equipment (constant injection volume 100 μL). SEC measurements of the diluted aliquots were triplicated. SEC data were collected and processed using OmniSEC software (Malvern, v. 5.12).

Normalization of the constant values of the SEC detectors (RI, LS, IV) was performed using PEO standards for triple calibration PolyCAL™ TDS-PEO-N (M_w 24 kDa, Malvern) at a concentration of 2.468 mg/mL.

S1.2. Nuclear magnetic resonance (NMR) measurements. The NMR experiments were conducted at a temperature of 22 °C using a Bruker Ascend™ 400 MHz spectrometer (Bruker). ^{1}H NMR measurements were performed employing a 90° single-pulse sequence for 128 scans with a 5 s recycle delay. ^{1}H NMR spectra of p(METAC-*stat*-PEO$_{19}$MEMA) copolymers with three different compositions were recorded in D$_2$O. The concentration of the samples was 20 mg/mL.

S1.3. X-Ray diffraction (XRD) measurements. Crystalline phase of the particles was identified by performing powder XRD measurements on a Bruker D8 Advance da Vinci design diffractometer working using parallel beam geometry.

S1.4. Scanning electron microscope (SEM) measurement. The morphology and size of sintered $GdPO_4$ particles was investigated using scanning electron microscopy (SEM). SEM images were taken with high-resolution scanning electron microscope (FE SEM) Hitachi SU-70, with accelerating voltage up to 10 kV. Samples for SEM were prepared by dispersing particles in distilled water and adding 20 μL of aqueous dispersion on a Si plate.

S1.5. TEM measurements. For morphology, size, shape and coating evaluation, FEI Tecnai F20 X-TWIN transmission electron microscope (TEM) was used. Measurements were carried out using 200 kV accelerating voltage, images obtained by using Gatan Orius CCD camera.

S2. Controlled hydrothermal synthesis of $GdPO_4$ particles with different morphology.

S2.1. Synthesis procedure. $Gd(NO_3)_3$ (0.5 mL, 0.4 mmol) was dissolved in 20 mL of deionized water and stirred for 15 min. Later, tartaric acid (1.20 g, 8 mmol) dissolved in 20 mL of deionized water was dropwise added to $Gd(NO_3)_3$ solution and allowed to stir for additional 30 min at room temperature to form Gd-tartaric acid complex. After complex formation the pH value of aqueous mixture was set to 10 by using ammonium hydroxide. Then, required amount of $NH_4H_2PO_4$ (depending on desired morphology of the particles to be obtained) was dissolved in 20 mL of deionized water and added dropwise into solution of Gd-tartaric acid complex, under vigorous stirring. The volume of reaction mixture was adjusted to 80 mL by adding distilled water. Afterwards, the mixture was poured into Teflon bottle autoclave, sealed and placed into hydrothermal reactor (*Berghof*) equipped with BTC-3000 Temperature Controller and Data Logger (*Berghof*) for 12 h at 160 °C temperature. Finally, the reaction product was separated by centrifugation at 7500 rpm (centrifuge model Eppendorf 5804), and washed four times with deionized water, dried to constant weight under reduced pressure at 40 °C.

S2.2. Crystallographic data. After performing X-ray diffraction analysis synthesized $GdPO_4$ particles were identified to possess rhabdophane crystalline phase. Reference card No. PDF ICDD 00-039-0232.
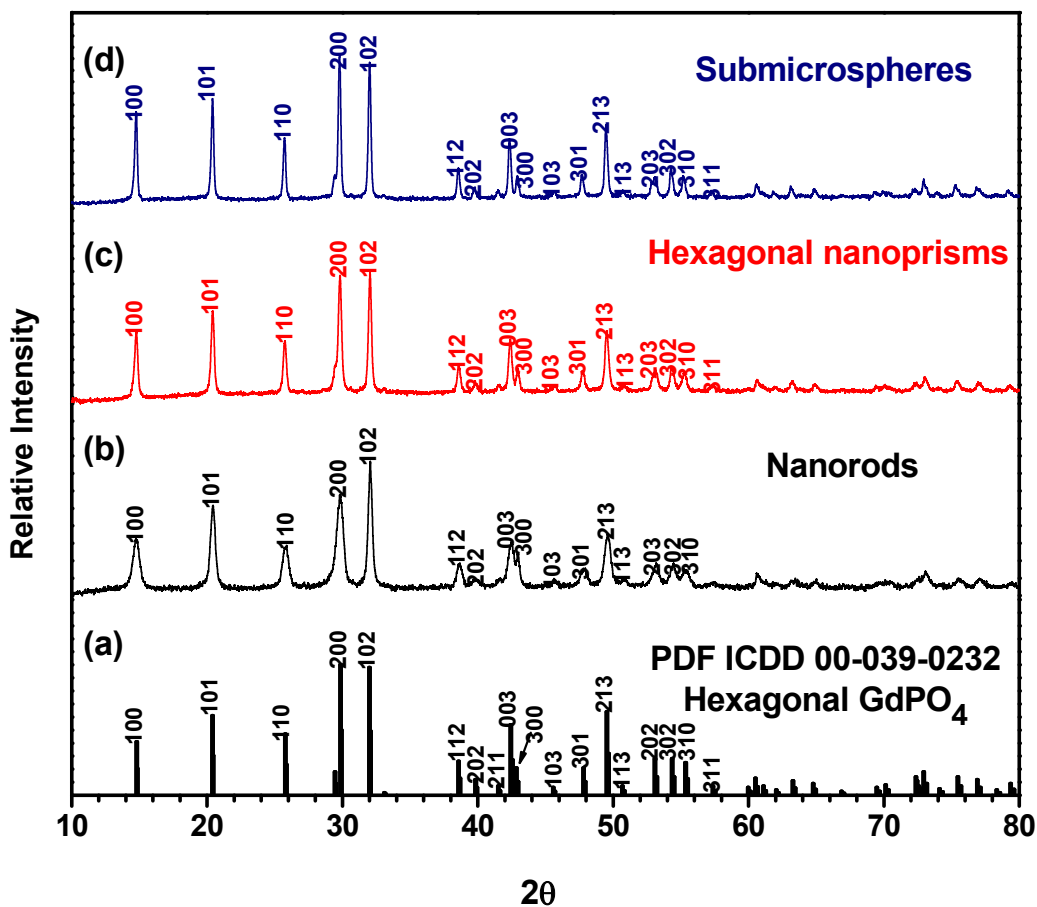

Figure S1. XRD patterns of synthesized $GdPO_4$ particles with different morphology: nanorods (b), hexagonal nanoprisms (c), submicrospheres (d); XRD reference pattern of $GdPO_4$ (a).

S3. Investigation of synthesized cationic brush-type polyelectrolytes

S3.1. SEC data. Molecular weight distribution (MWD) curves of p(METAC-*stat*-PEO$_{19}$MEMA) samples with different composition is presented in Fig. S2. The unimodal distribution of molecular weight and low dispersity proves a well-controlled character of the RAFT polymerization process.
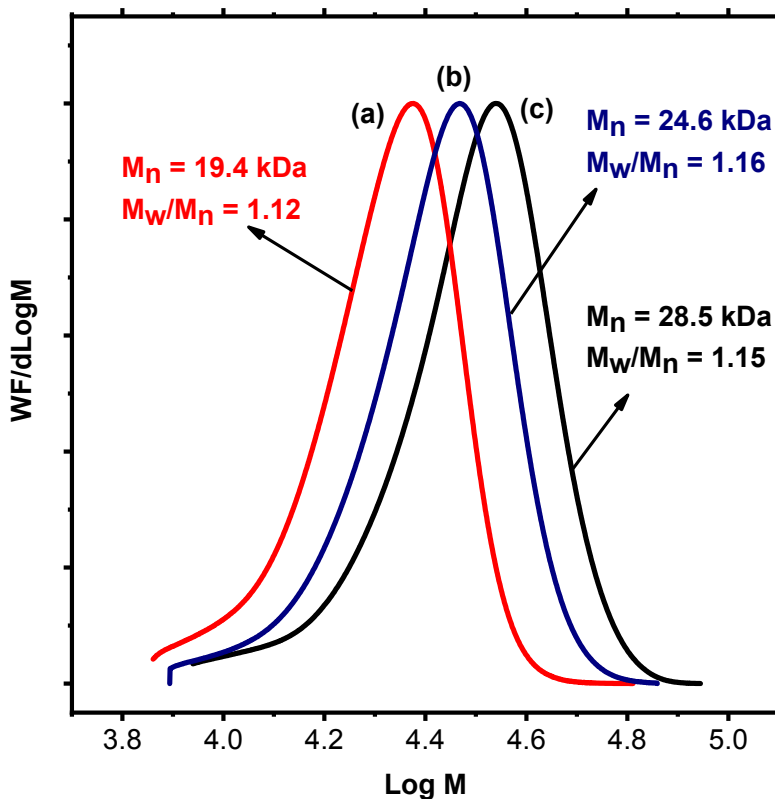

Figure S2. Molecular weight distribution curves of synthesized p(METAC-*stat*-PEO$_{19}$MEMA) containing different charge density (different amount of METAC monomeric groups in composition): 65 mol % (high, (a)), 47 mol % (medium) (b)) and 27 mol % (low (c)).

S3.2. NMR data. The structure of synthesized p(METAC-*stat*-PEO$_{19}$MEMA) copolymers were proved from ^{1}H NMR spectra (Fig. S3). The exact composition was calculated by comparing integrals of typical peaks of each monomer (see magnified area in Fig.S3) using Eq. S1:

$$F_1 = \frac{\frac{1}{3}\int 3.26}{\frac{1}{3}\int 3.26 + \int 3.35} \times 100 \qquad \text{(S1),}$$

where F_1 – the positive charge containing ammonium groups (of METAC monomer) in copolymer composition (mol %), $\int 2.26$ and $\int 3.35$ represent the integrals of chemical shift of $-N(CH_3)_3$ (*9H*) groups (in METAC) and $-OCH_3$ (*3H*) groups in PEO$_{19}$MEMA, respectively.
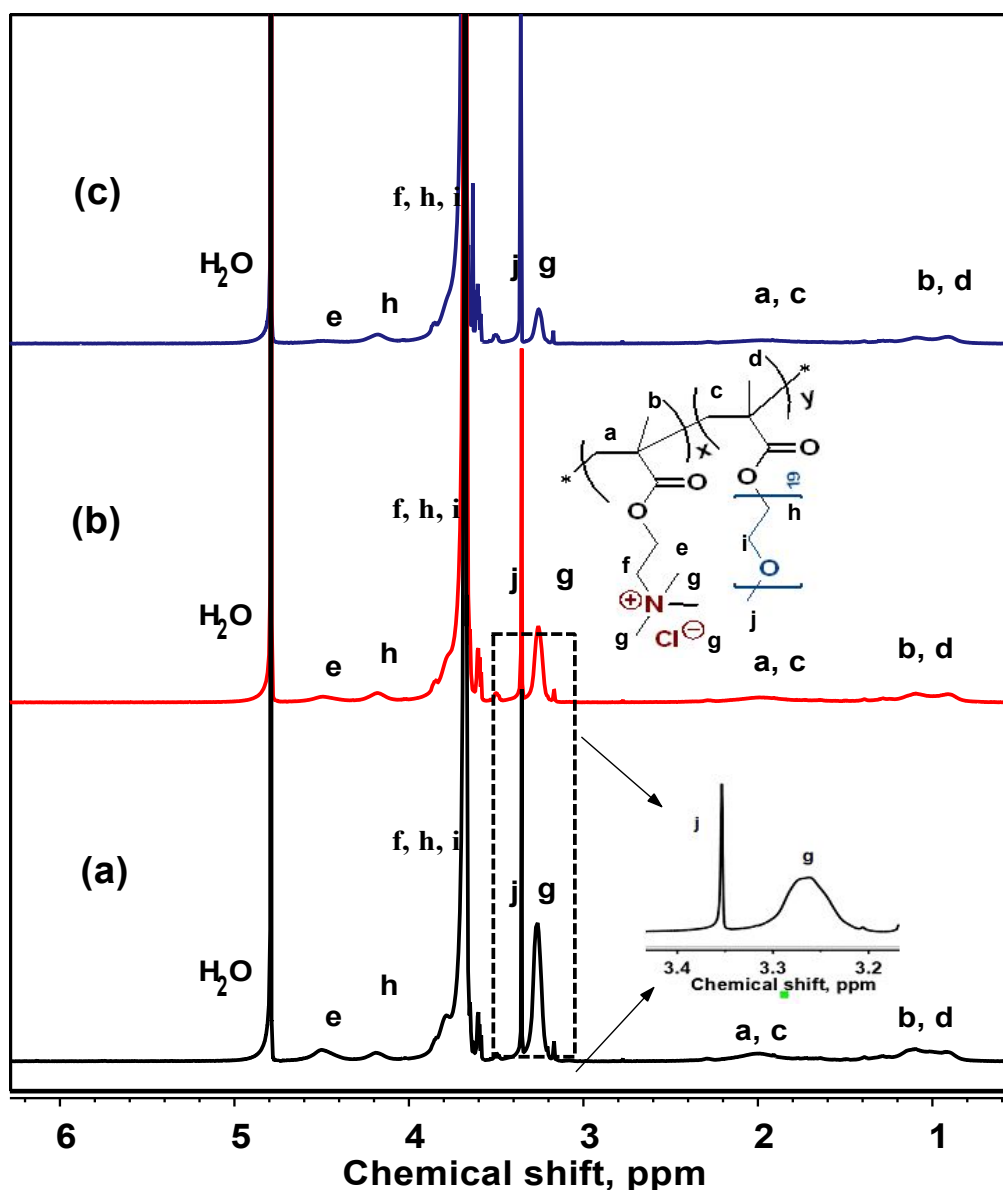

Figure S3. ^{1}H NMR spectra of p(METAC-*stat*-PEO$_{19}$MEMA) with high (a), medium (b), and low (c) charge density.

S4. Stability of GdPO$_4$ particles in biological aqueous media.
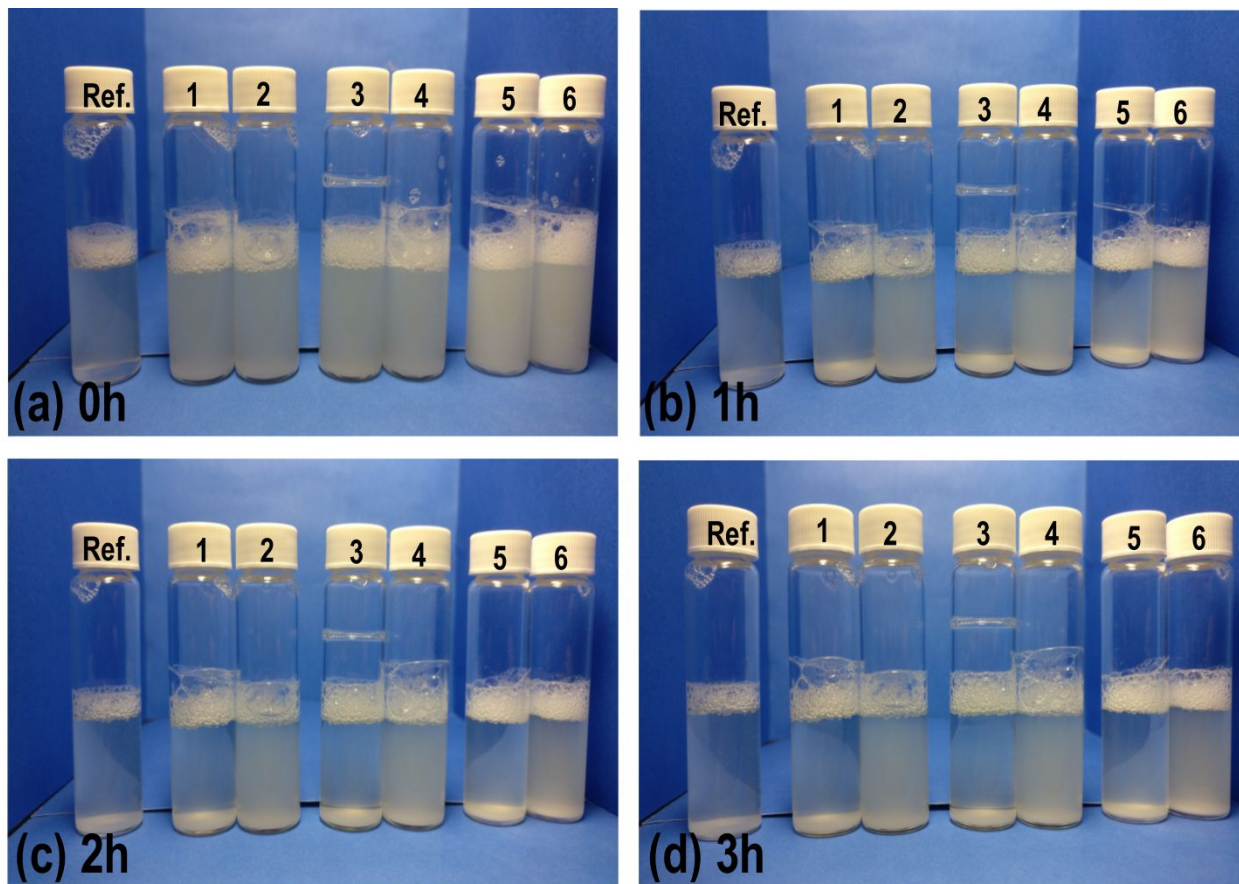
Figure S4. Visual evaluation of GdPO$_4$ particles ((nanorods (1 bare, 2 modified), hexagonal nanoprisms (3 bare, 4 modified), submicrospheres (5 bare, 6 modified)) stability in biological aqueous media (consisting 10 vol. % human blood plasma, pH 6.5 (Ref.)) over time: (a) 0 h; (b) 1 h; (c) 2 h; (d) 3 h.
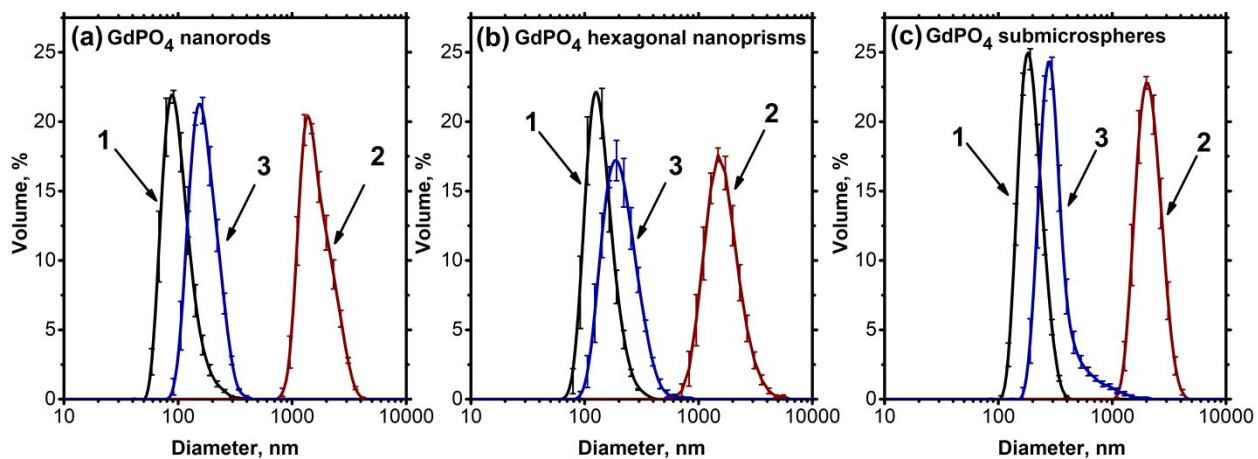
Figure S5. Particle size distribution in aqueous dispersions (pH 6.5) of GdPO$_4$ particles with different morphologies (nanorods (a), hexagonal nanoprisms (b) and submicrospheres (c)) after incubation in protein-rich aqueous media (consisting 10 vol. % human blood plasma, pH 6.5). 1 − the initial PSD; 2 – bare particles; 3 – modified particles.